

University of New Mexico

UNM Digital Repository

Physics & Astronomy ETDs

Electronic Theses and Dissertations

5-31-1967

Analysis of Particle Counting Rate Variations Observed on Satellite OSO-B2

Esther Y. Ma

Follow this and additional works at: https://digitalrepository.unm.edu/phyc_etds



Part of the [Astrophysics and Astronomy Commons](#), and the [Physics Commons](#)

Recommended Citation

Ma, Esther Y.. "Analysis of Particle Counting Rate Variations Observed on Satellite OSO-B2." (1967).
https://digitalrepository.unm.edu/phyc_etds/288

This Thesis is brought to you for free and open access by the Electronic Theses and Dissertations at UNM Digital Repository. It has been accepted for inclusion in Physics & Astronomy ETDs by an authorized administrator of UNM Digital Repository. For more information, please contact disc@unm.edu.

UNIVERSITY OF NEW MEXICO LIBRARY

MANUSCRIPT THESES

Unpublished theses submitted for the Master's and Doctor's degrees and deposited in the University of New Mexico Library are open for inspection, but are to be used only with due regard to the rights of the authors. Bibliographical references may be noted, but passages may be copied only with the permission of the authors, and proper credit must be given in subsequent written or published work. Extensive copying or publication of the thesis in whole or in part requires also the consent of the Dean of the Graduate School of the University of New Mexico.

This thesis by Esther Y. Ma
has been used by the following persons, whose signatures attest their acceptance of the above restrictions.

A Library which borrows this thesis for use by its patrons is expected to secure the signature of each user.

NAME AND ADDRESS

DATE

ANALYSIS OF PARTICLE COUNTING RATE
VARIATIONS OBSERVED ON SATELLITE OSO-B2

By

Esther Y. Ma

A Thesis

Submitted in Partial Fulfillment
of the Requirements for the Degree of
Master of Science in Physics

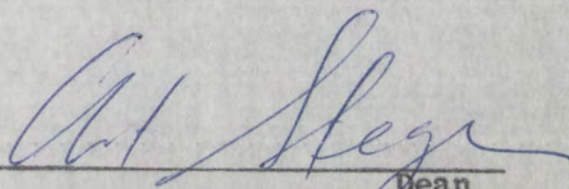
The University of New Mexico

1967

LD
3781
N563M111
COP.2

This thesis, directed and approved by the candidate's committee, has been accepted by the Graduate Committee of the University of New Mexico in partial fulfillment of the requirements for the degree of

MASTER
OF
SCIENCE

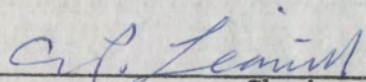

Dean

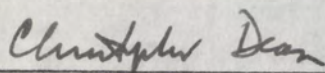
Date 5-31-67

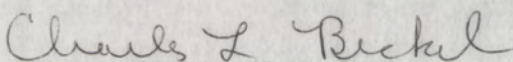
ANALYSIS OF PARTICLE COUNTING RATE
VARIATIONS OBSERVED ON SATELLITE OSO-B2

Esther Y. Ma

Thesis committee


Chairman





435163

TABLE OF CONTENTS

	Page
Abstract	1
Acknowledgement.	2
Introduction	3
The Experiment	5
Discussion of Geomagnetic Effect	8
Discussion of Satellite Effect	12
Experimental Results and Interpretation.	14
Correlation with the Solar Activity.	20
Figures 1 - 29	23
References	53

ABSTRACT

The ommidirectional cosmic ray fluxes at an altitude of 300 miles and within ± 34 degrees latitude were studied using two Cerenkov counters and a scintillation counter aboard the OSO-B2 Satellite. The fluxes were found to depend strongly on the geomagnetic field with the trapped particles in the South Atlantic Radiation Anomaly being directional in some locations.

ACKNOWLEDGEMENTS

I would like to express my appreciation to Dr. C. P. Leavitt for his invaluable assistance and guidance in the preparation of this thesis.

INTRODUCTION

Since the discovery of cosmic rays by Wilson in 1900, many scientists have tried to discover their origin, composition, characteristics and variations.

One of the characteristics of the cosmic rays is their constancy in time. The analyses of the content of the C^{14} and H^4 produced as a result of cosmic ray bombardment, in different layers of the earth, has indicated that the flux of cosmic rays in the vicinity of the earth and solar system has not varied by more than 10 to 20 percent over the last 30 centuries. The local and transient deviation from the constancy is very important since it provides information on such problems of astrophysics and geophysics as the mechanism of production of the cosmic rays, their place of origin, the mode of propagation to earth and the influences on them arising from the electromagnetic conditions of interplanetary space and the sun.

The causes of the time variation of the primary cosmic rays, cosmic rays incident upon the top of the atmosphere of the earth, have been distinguished as:

1. Solar diurnal variation due to a spatial anisotropy of the radiation and the rotation of the earth.
2. Presence of a source whose intensity varies with time such as the sun during the solar flare activity.
3. The modulation effects associated with the magnetic storms, also called Forbush Decreases.

4. Long term change in cosmic ray intensity which is anti-correlated with the 11 year solar activity cycle, and is thus called the 11 year variation.

Experiments (Dainton 1951) have shown that most of the primary cosmic rays are protons. The remainder are α -particles, heavier nuclei, 1 percent electrons and 0.1 percent γ -rays.

According to the electromagnetic mechanism (Störmer 1951), the charged particles of the cosmic ray flux would be deflected by the geomagnetic field. Therefore, in the time variation observation, geomagnetic effects should be considered.

In addition to the primary radiation, particle detectors above the earth's atmosphere respond to the fluxes due to particles, mostly protons and electrons, trapped in the earth's magnetic field. These particles must be considered as distinct from the primary cosmic radiation since their characteristics are determined entirely by injection and loss mechanisms near the earth. Typically the particles have lower energies and much higher fluxes than the primaries. Time variations in the trapped radiation result from solar-induced geomagnetic disturbances and direct solar particle injection.

Satellites have been used very often recently in primary cosmic ray observations and in measurements of the trapped radiation.

An important problem in investigating time variations is the separation of the various instrumental effects superimposed on them. This is especially true in satellite observations because of the changing position and orientation of the detectors. In this investigation, time

variations observed in counting rates of satellite-borne detectors are analysed in an attempt to separate true variations in particle flux from geographical effects and fluctuations arising from the spin of the spacecraft in anisotropic flux fields.

THE EXPERIMENT

While the primary purpose of the experiment was the investigation of galactic gamma rays, the individual counters measured the integrated fluxes of electrons and protons with energies higher than the detector thresholds. It is the response of these counters that will be analysed for time variations in this paper.

THE SPACECRAFT:

The experiment took place on the Orbiting Solar Observatory (OSO-B₂) satellite which was launched in February 1965 and was orbiting around the earth at the altitude of approximately 300 nautical miles. The eccentricity was very close to zero. The apparent precession per orbit was 25 degrees west, the inclination to the equator was approximately 33 degrees, and the period was about 95 minutes. A plot of the nominal orbit is shown in Figure 1.

The structure of the satellite included a wheel of aluminum alloy material and a fan-shaped sail. The wheel was separated into nine wedge-shaped compartments. Five of these compartments contained apparatus

for non-pointed experiments, and the rest housed the control, telemetry, radio command equipment and batteries. The sail, mounted on top of the wheel by means of a rotating shaft, carried the solar cell array and pointed experiments. The configuration of the satellite is illustrated in Figure 2. The wheel spun about the axis with the rate of 30 ± 1.5 rpm. The spacecraft was maintained in a position so that the spin axis was normal to the sun vector within $\pm 3^\circ$.

The OSO-B₂ employed a PCM/PM telemetry system. The data was time-multiplexed into 8 bits per word and 32 words per main frame. The spacecraft simultaneously tape recorded and transmitted real-time data at a rate of 400 bits per second (0.64 sec. per main frame). Among the 32 main frame words five were used for the spacecraft and experiment housekeeping data, three were used for the sail and two for the wheel. Two forty-eight channel commutators, one located in the sail and another one in the wheel, were used to process subcommutated analogue housekeeping data, monitoring the status of the sections into five main frame words. The data of the experiment measuring the gamma ray flux used two main frames (for the energy of the particle and the orientation of the compartment in which the instrument was housed) and three channel commutators (for individual detector rates; channel 4 for the counting rates of the scintillation counter, channel 3 for the lead-glass cerenkov counter and channel 2 for the lucite cerenkov counter). Because of this arrangement, the readout time of the New Mexico main frame words was once per 0.64 second and once per 15.36 seconds for the three analogue channels. The tape-recorded data were

commanded to play back once per orbit, taking approximately 5.5 minutes. During this play back interval, the real-time data were neither transmitted nor recorded (NASA-GSFC Operations Plan 1964).

THE INSTRUMENT:

The instrument included a scintillation counter, a lead-glass cerenkov counter and a lucite cerenkov counter. All the counters were connected with photomultiplier. The arrangement of the instrument is shown in Figure 3.

The sensitivities of the counters are not accurately known, but for the scintillation counter, it could be assumed (Birk 1953) to be 100% when the energy of the detected particle is higher than the threshold energy.

The threshold of the scintillator was supposed to be 0.35 Mev. Due to a possible photomultiplier gain drift it was assumed to be 2 Mev. The threshold energy of the cerenkov process was a function of index of refraction, which is 1.47 for lucite and 1.67 for lead-glass; hence the threshold energies are 200kev and 140kev for electron while 320Mev and 230Mev for proton (Jelley 1958). The photomultiplier thresholds were 6.2 Mev and 9 Mev for the lucite and lead-glass counters.

As was shown in Figure 3, before the particles impinged on the counters it might be necessary for them to pass through the aluminum wheel housing, the lucite light pipe and the skin of the counter. The threshold, which then would depend on the path of the particle, might be greatly increased. By knowing the absorption energy (by ionization and radiation) of lucite and aluminum from electrons and protons (Jelley 1958) the minimum energy for penetration (normal incident particles) then can be found.

DISCUSSION OF GEOMAGNETIC EFFECT

Because the satellite position varies rapidly with time, geographical variations in particle fluxes will appear as time variations. It is therefore necessary to discuss the various effects which cause fluxes to vary with position. If the non-solar cosmic flux in space is normally isotropic the magnetic field of the earth will be responsible for geographical variations.

According to Liouville's Theorem, in a steady magnetic field the density of the cosmic rays in the phase space is conserved. Along the trajectory of the particles the directional differential intensity, number of particles with momentum between p and $p \pm dp$ which cross an element dS in time dt and contained in a solid angle $d\Omega$, is constant in time. If the intensity of particles at infinite distance from the earth is isotropic, then the intensities at any point and any direction near the earth should be the same as they are at infinity. However, since the earth's magnetic field, which depends on geographic position, can exclude particles below a field-dependent cut-off energy, the total cosmic ray intensity exhibits a geographic variation.

Considering the geomagnetic field as a field set up by a centered dipole, it can be shown (Hooper 1965) that particles with rigidity, $\frac{pc}{ez}$, less than a critical value (cut-off rigidity) can not reach the earth at any direction. This value was defined by Störmer as:

$$r_c = \frac{M}{R^2} \frac{\cos^4 \lambda}{(g^2 - \sin \theta \cos^3 \lambda + g^2)^2},$$

where M is the moment of the equivalent dipole (8.1×10^{22} amp-meter²),

λ is the geomagnetic latitude, R is the distance from the dipole center of the particle, θ is the angle between the path of the particle and the projection of the earth on a meridian plane, and g is a constant dependent upon the angular momentum of the particle at infinity about the axis of the dipole. Table 1 shows the variation of g at different latitudes (Janossy 1948).

Table 1

λ	0°	10°	20°	30°
g	0.978	0.911	0.806	0.783

According to Störmer, for particles with rigidity larger than the critical value all directions were completely allowed. The condition of the critical rigidity was the boundary of the so-called Störmer cone, in which all directions were allowed. In Störmer Theory it was assumed that the earth permitted particles to pass through it without suffering any absorption. By removing the above assumption, Lemaître and Vallarta found that inside the Störmer cone there is a penumbra region in which directions are partly forbidden. The vertical ($\theta = 0^\circ$) cut-off rigidity as a function of geomagnetic latitude is shown in Figure 4. Experiments (Schwartz 1956) have shown in the high latitude area (geomagnetic latitude $\geq \pm 50^\circ$), the flux intensity does not change with the latitude. As was shown in

Figure 1, the satellite orbits were confined within geographic latitude $\pm 34^\circ$ which corresponds to a region within geomagnetic latitude $\pm 46^\circ$. Therefore, the constant flux intensity phenomenon will not be discussed.

Besides the dependence on the geomagnetic latitude, the intensity of the charged particles in the cosmic rays also has its longitude and asymmetry effect.

The reason for the longitude effect was found to be that the geomagnetic center (center of the assumed dipole) does not coincide with the geographic center. The distance of an observer at the geomagnetic λ on the geomagnetic equator from the geomagnetic center would be

$$R_0^2 = R_E^2 + \epsilon^2 - 2R_E\epsilon \cos(\lambda - \lambda_0).$$

Where ϵ is the distance between the dipole center and the geographic center ($\epsilon \simeq 300$ km), and R_E is the average earth radius. λ_0 is the geomagnetic longitude of the point on the equator which is nearest to the geomagnetic center. Therefore, the cut-off rigidity on the geomagnetic equator is

$$r_c(\theta = 0, \lambda) = \frac{M}{R_E^2 + \epsilon^2 - 2R_E\epsilon \cos(\theta - \theta_0))(\sqrt{1 - \sin^2\theta} + 1)^2}.$$

It was found that the cosmic ray intensity inclined at an angle η to the west from the vertical is larger than the corresponding intensity from the east. This is the east-west asymmetry effect. This effect was proven to be the result of the primary cosmic ray flux

containing an excess of particles of positive charge.

An asymmetry between north and south was also observed. This has been described by Lemaitre and Vallarta as due to the peculiar shape of the allowed cone.

The abnormally weak geomagnetic field (negative) near the South Atlantic Ocean region lowers the mirror points of the trapped particles in the Inner Van Allen Belt above this area and forms the South Atlantic Radiation Anomaly (SARA) at an altitude between 220 km to 700 km (Dessler 1959). From experiments and numerical calculation (Hess 1965) it can be shown that the main source of the trapped particles could be the solar wind and the beta-decay of neutrons produced by the cosmic ray proton colliding with oxygen and nitrogen nuclei. The intensity of the trapped particles is very steady. Therefore, there should also be a loss process. Protons are lost by ejection into the atmosphere after their energy becomes very low through inelastic nuclear collisions with the atmosphere or by charged exchange with slow protons. Since electrons are much lighter, for the same momentum, the energy of electrons is much lower than that of protons. Through coulomb scattering they are easily scattered into the atmosphere.

DISCUSSION OF SATELLITE EFFECT

Frequently the spin of the satellite will introduce periodic fluctuations in the counting rates. Obviously directional detectors and directional fluxes are required. In this experiment, such periodic fluctuations were observed, which are very unlikely to be due to inherent time variations in the fluxes. That these fluctuations represent space periodicity is also unlikely but it is of interest to analyse them to be sure that they are consistent with the assumption that they were produced by the satellite spin. In addition it may be possible to obtain information about the directional characteristics of the radiation and especially about the time variation of these characteristics.

The proton and electron flux was read out once every 15.36 second; therefore, the appearance of the data recorded is strongly dependent on the relation between the spin rate and the read-out rate. This dependence should be clarified first.

Let T be the observed period of the counting rate of the flux

τ be the read-out period (15.36 sec.)

T_s be the true counting rate period due to the spin effect of the satellite and the characteristics of the flux

then
$$\tau = \frac{nT_s}{2} \pm t .$$

Where n can be zero or any positive integer, t is the time difference between $\frac{nT_s}{2}$ and the read-out period corresponding to a phase change which is greater than or equal to $\frac{\pi}{2}$.

therefore $T = \frac{2 \cdot T_s}{2 - nT_s}$ when n is an even integer. When n is an odd integer T does not equal to $\frac{2\pi}{\delta}\tau$ exactly, the amplitude of the observed counting rate instead of being a constant will be changed by a modulating factor.

After the read-out effect has been removed the appearance of the data still depends on factors such as the relative direction of the spin axis to the direction of the flux, and the directional characteristics of the counters, besides the time and space variations of the flux. Away from the SARA the range of the energy of the charged particles is so great that the directions of the particles as they were mentioned in the geomagnetic effect will be too random to be analysed. In the anomaly most of the charged particles were particles with lower energy and were trapped by the magnetic field; the directions of the flux are much more coherent than those in other regions.

In the SARA if the particle flux was isotropic in space the data recorded would not be affected by the spin of the satellite. If the particles were undergoing the mirror reflection process so that their motion was mainly perpendicular to the magnetic field lines, the orientation of the spinning satellite wheel could result in the exposure of the counters to the radiation twice per revolution. On the other hand, if the particle fluxes were unidirectional, then the counters would be exposed once per revolution. If the response of the counter followed a sine function form, generally, the observed counting rate would be

$$Y_0 = Y_1 + Y_2 \sin 2\pi(\tau n/T_s) + Y_3 \sin 2\pi(2\tau n/T_s).$$

where Y_1 , Y_2 and Y_3 were the counting rates due to the space isotropic flux, the plane isotropic flux and the unidirectional flux respectively.

In order to concentrate on the subject of this chapter the small isotropic background which consisted of gamma-ray low energy protons and electrons was omitted.

$$Y_0 = Y_2 \sin 2\pi(\tau n/T_s)$$

and $Y_0 = Y_2 \sin 2\pi(2\tau n/T_s)$

were plotted with the value of T_s varied from 1.71 second to 2.20 seconds. Figures 5a and 5b are two among the ten plots. From these simulated curves the spin effect of the satellite on the data can be seen more clearly.

EXPERIMENTAL RESULTS AND INTERPRETATION

Nominal orbital data are shown in Figures 6-11. By using the data which were taken from February to July 1965, the world map and the time schedule, the counting rates of the three individual detectors at a certain position (within ± 5 degrees longitude and ± 2 degrees latitude) and time (± 0.5 minute) could be found. In Figure 6, a region of greatly increased counting rate is evident. From the world map data it was determined that the enhancement occurred in the South

Atlantic Region. This phenomenon is the South Atlantic Radiation Anomaly (SARA) which is associated with a magnetic anomaly as previously discussed.

THE OVERALL INTENSITY:

Figures 12 and 13 are two among the nine flux intensity-verses-time curves which were obtained from data reduced from the orbital data during the life time of the satellite. All of these curves indicated a decrease in flux intensity. This effect could be explained by the activity of the phototube. When the tubes are away from the light the noise level will die down gradually, thus giving a smaller contribution to the observed rate as time goes on. Therefore, the later data would seem to be the more reliable.

AWAY FROM THE ANOMALY:

Figure 6 indicates that outside the anomaly the counting rates of the scintillation counter and the lucite cerenkov counter were very low. Therefore, only channel 3 (lead-glass cerenkov counter) has been graphed in subsequent treatment of these regions.

According to the discussion in the preceding chapter, variations of the proton and electron flux at different latitude and longitude were expected.

Geographic Longitude Effect. The longitude effect has been studied along the geographic equator. The plots of counting rate against the longitude are shown in Figures 14a and 14b. The error of the plotting data was 5 percent which covers up most of the longitude effect, except it can still be seen that the counting rate around -120°

west is higher than the rest.

Geographic Latitude Effect. The results are shown in Figures 15a, 15b and 16. Both 15a and 15b indicate that the lowest intensity flux was located near the equator. The asymmetry of Figures 15 and 16 indicates that the geographic equator is not a curve of symmetry to the flux. In Figure 16 (longitude = 120° east) the highest intensity is located at the south while in Figure 15a (longitude = -120° west) the highest intensity is at the north. This phenomenon indicates that the geomagnetic poles are located in the south-east and the north-west geographically.

The Geomagnetic Effect. A world map with geomagnetic coordinates, set up by the centered dipole field, superposed on geographic coordinates is shown in Figure 17. The relation between these coordinate systems is given (Janossy 1948, Webb 1958 and Hopper 1965) as

$$\begin{aligned}\sin \lambda &= \cos 78.3^{\circ} \cos \theta \cos (\varphi - 291^{\circ}) + \sin 78.3^{\circ} \sin \theta, \\ \cos \Lambda &= (\sin 78.3^{\circ} \cos \theta \cos (\varphi - 291^{\circ}) - \cos 78.3^{\circ} \sin \theta) / \cos \lambda, \\ \tan \varphi &= \tan (\Lambda + 69^{\circ}) \sin k / \sin (k - 11.5^{\circ}),\end{aligned}$$

and $\tan \theta = \cos \varphi \cot (k - 11.5^{\circ}).$

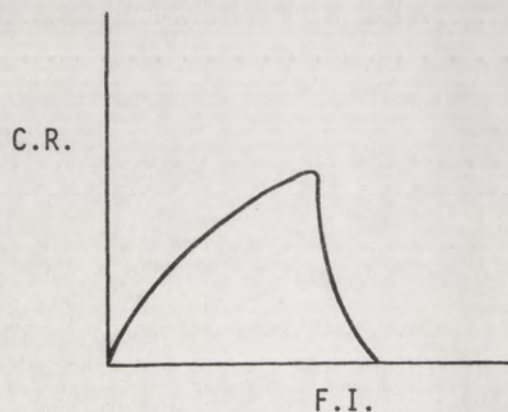
Where λ is the geomagnetic latitude,
 Λ is the geomagnetic longitude,
 θ is the geographic latitude,
 φ is the geographic longitude.

The world maps used for analysis were converted into geomagnetic world maps. The dependence of the flux intensity on the geomagnetic coordinates is shown in Figures 18 and 19.

Geomagnetic Longitude Effect. Figure 18 does not show any effect due to the variation of the longitude along the geomagnetic equator. The points rather than being in a narrow band, have a spread which is larger than the experimental error would indicate. The effect could be due to neglect of the deviations of the actual magnetic field from that of a simple centered dipole.

Geomagnetic Latitude Effect. In Figure 19 the latitude effect is quite symmetrical with respect to the magnetic equator. This plot was taken from geomagnetic longitude 296 ± 1 degrees, at which previous experiments have been shown that cosmic rays equator is very close the dipole field equator (Savenko 1962).

IN THE ANOMALY Examining the orbiting data in Figures 6-8, it was found that in one part of the anomaly there were no data. This was because in that part of the anomaly the flux intensity of the charged particles was so high that the phototube became saturated and no data were recorded. The relation between the flux intensity and the counting rate is not single-valued as is shown in the following graph. Therefore, when the flux is very high the increase of the flux can cause a decrease of the corresponding counting rate. This could



explain the large variations near the center of the anomaly. In Figure 11 the silent spot was located in an area away from the anomaly and was due to the fact that satellite playback was taking place. Figure 20, an energy spectrum of proton in the SARA, indicates that there are very few protons which have energy above threshold. Consequently, the cerenkov counters mainly served as electron counters in this area. In Figures 8-10 the overflowing only happened to the scintillation counter in the middle of the anomaly while the data of the cerenkov counters indicate that at the altitude of about 300 nautical miles in the SARA the electron flux (above threshold) is shifted toward the west. From the quick-look data the accurate spin period of the satellite has been calculated. The average value of it in an arbitrary orbit was 1.94 seconds. The instantaneous value varied within ± 0.8 second. Figures 9-10 indicate that at the border of the anomaly the counting rate of the scintillation counter has very interesting variations. Since the read-out period was 15.36 seconds all the periods of the variation should be an integer (no less than 2) multiple of this time interval. It is observed that the periods of the variations near the eastern border were mostly 2τ as compared to 4τ at the west. The spin rate should change as the satellite enters the day or night time. During the orbits of Figures 9-10 the satellite was not in the anomaly at those very moments so that it could be assumed that the spin rate was constant in the anomaly. The doubling of the variation period could be due to the directional fluxes. Comparing the orbiting data near the border of the anomaly with the simulating curves in Figures 5a and 5b, it was found that the variation in the

west was similar to the simulating curve with spin period equal to 1.98 seconds while on the other side it was similar to the one with the period equal to half of the above value. According to what have been mentioned in the Satellite Effect, this could be explained if some of the fluxes recorded in the east were in planes which were perpendicular to the field lines and some of those recorded in the west were unidirectional fluxes. It will be noted that the simulating curve whose spin period is 0.990 sec. is modulated; that this effect has not been observed in the orbiting data could be due to the brevity of time interval of the satellite passage through the border area. In Figure 8 is shown one of the orbits in which the counting rate at the western border did not have periodic variation. This may be due to the effect of the satellite spin orientation with respect to the particle directions, or it may indicate that the combination of trapped and precipitating radiation produced an effectively isotropic distribution. It should be noted that both precipitating particles (along the field lines) and mirroring particles (perpendicular to the field lines) exhibit symmetry about the field lines. It is therefore difficult to see how the orientation of the spin axis could permit periodic counter response in one case and not in the other. For example, for the case of mirroring particles the counters will show no spin-produced variation if the spin axis is along the field lines. But it is clear that in this situation the counters will not show periodic response to unidirectional radiation along the field lines also. Since the lack of periodic response is observed consistently on the west side of the anomaly, the more likely interpretation is that an effectively

isotropic flux can exist here at certain times. Another possible effect is the generation of large fluxes of bremsstrahlung by energetic electrons striking the spacecraft. If the counters never point in the direction of the electrons, their main response will be to the bremsstrahlung and will not exhibit directional variations. If this is the case, however, it requires that the directionality be of the type normally found in the west, that is, unidirectional, since particles in mirror distribution (in planes) cannot be avoided by counters located on a spinning spacecraft regardless of orientation.

THE CORRELATION WITH SOLAR ACTIVITY:

Because of the rather short life time of the satellite the long term change in cosmic rays which is anticorrelated with the solar activity could not be observed. Also due to the noise of the phototube the solar diurnal variations which are very small would not be expected to show.

During the life time there occurred several important solar flares. At the time of occurrence of a flare, the sun will emit a cloud or a stream of ionized matter, mostly hydrogen, which, travelling with velocity of 1,000 to 2,000 km/sec., will arrive at the vicinity of the earth at about 38 hours. As a result of its high conductivity, the plasma carries with it the magnetic field that was in the sunspot area where the flare originated. Forming a magnetic bottle (Gold 1965) around the earth (Figure 21), the new magnetic field inhibits the entrance of the lower energy galactic cosmic rays and causes the Forbush Decrease. The approaching of the plasma will also compress the original earth magnetic field and cause the magnetic storm which

starts with a sudden increase in the magnetic intensity (Sudden Commencement). Meanwhile, during a solar flare a lot of extra particles will be produced by the sun. Some of these particles may arrive at the earth as extra intensity of the cosmic rays.

According to the report from Lincoln (1965) there were nearly world wide observations of severe magnetic storm on April 17, 1965. Figures 22-25 are the data of the orbits which went through the same tracks but not during any magnetic storm.

As can be seen from the figures, there is no evidence for a Forbush Decrease. The decrease would have to be quite large to be detected because of the low counting rates and the short integration time. There was also no evidence for an increase due to solar particle injection into the radiation belts. This would be observed only during passage through the South Atlantic Anomaly since solar protons would be below the geomagnetic cut-off. A critical examination of the boundaries and intensities of the anomaly during flare activity failed to disclose any significant changes. Either any change had died out by the time the satellite traversed the anomaly, proton injection was confined to the outer belts, or solar protons did not impinge on the earth. It should be noted that certain high-flux regions of the anomaly were obscured consistently by satellite data drop-out.

By comparing Figures 22-25 and 26-29 it was found that the shape of the counting rates did not have significant difference except the size of the anomaly did indicate an increase corresponding to a

change of one to three minutes in the travelling time of the satellite. This could be explained if in the anomaly the flux intensity does not change as much as the area of the anomaly with the altitude since the impinging plasma following the solar flare will also lower the Inner Van Allen Belt.

Figure 1

Nominal OSO-B2 Satellite Orbit
in Geographic Coordinates

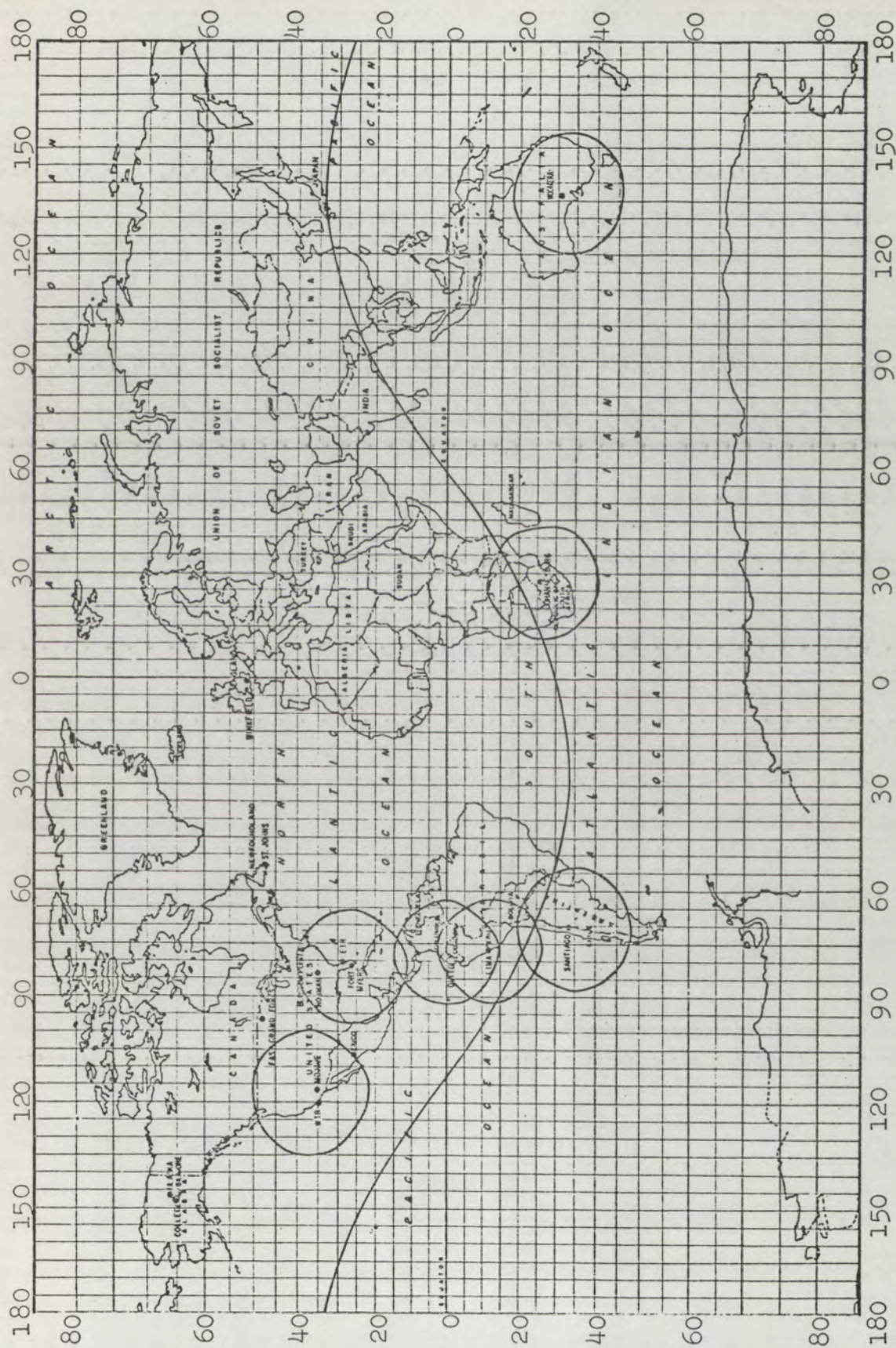


Figure 2

The Configuration of the Satellite OSO-B2

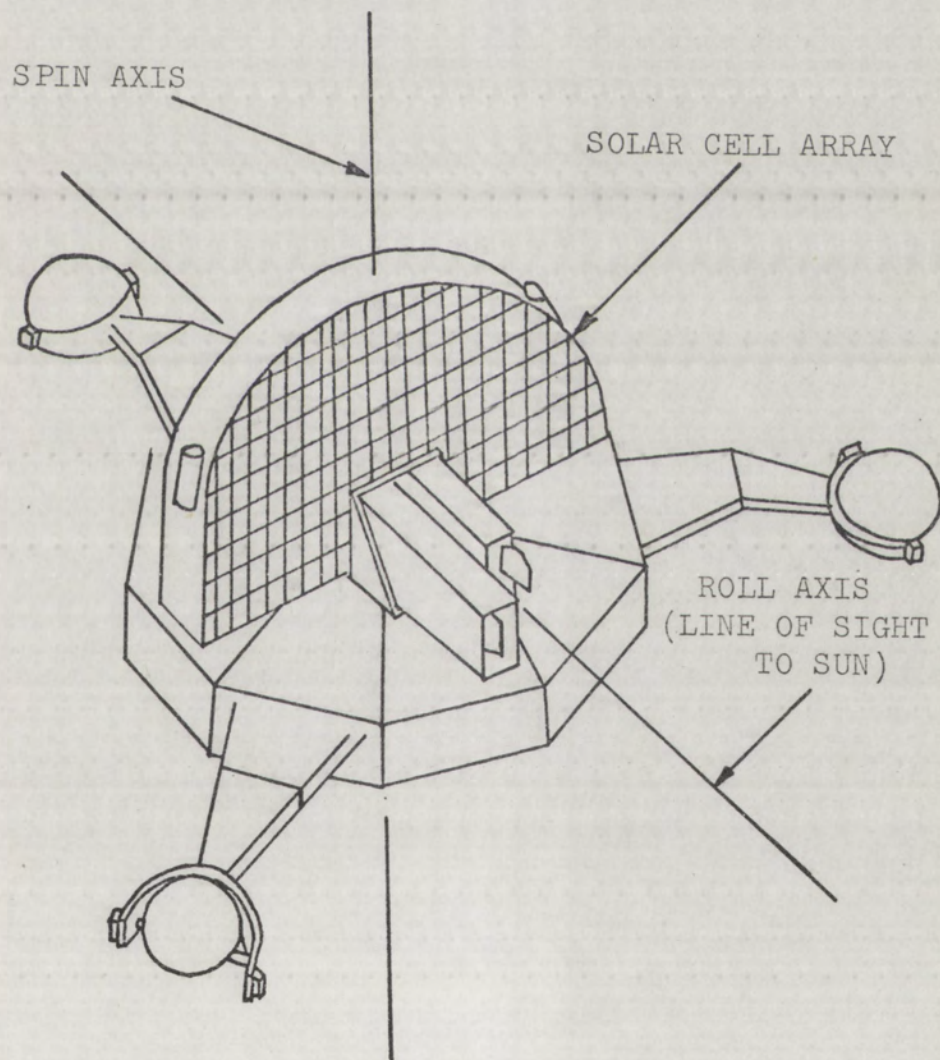


Figure 3

A Diagram of the Instrument

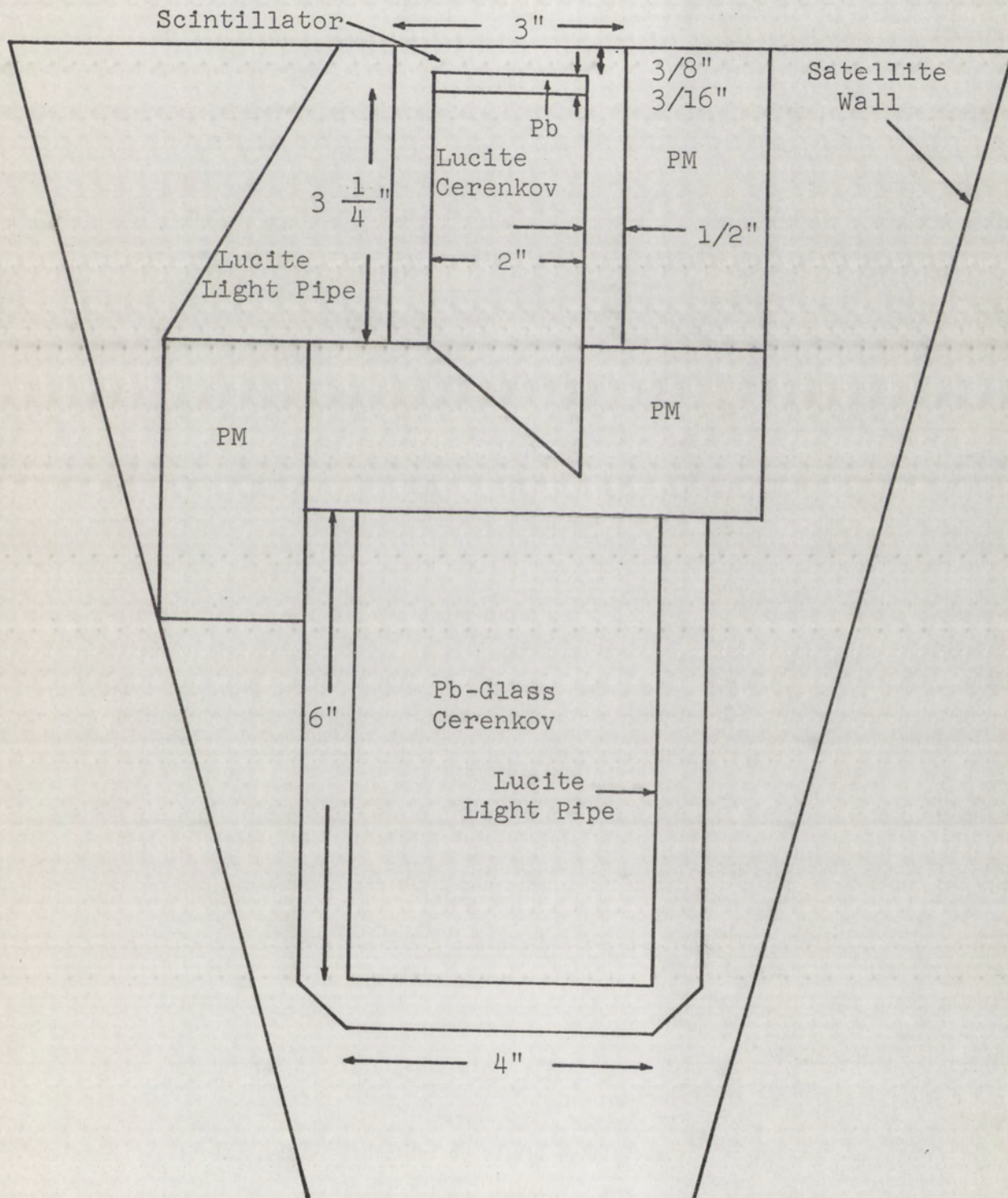


Figure 4

Cut-off Rigidity (in the Vertical Direction)
as a Function of Geomagnetic Latitude

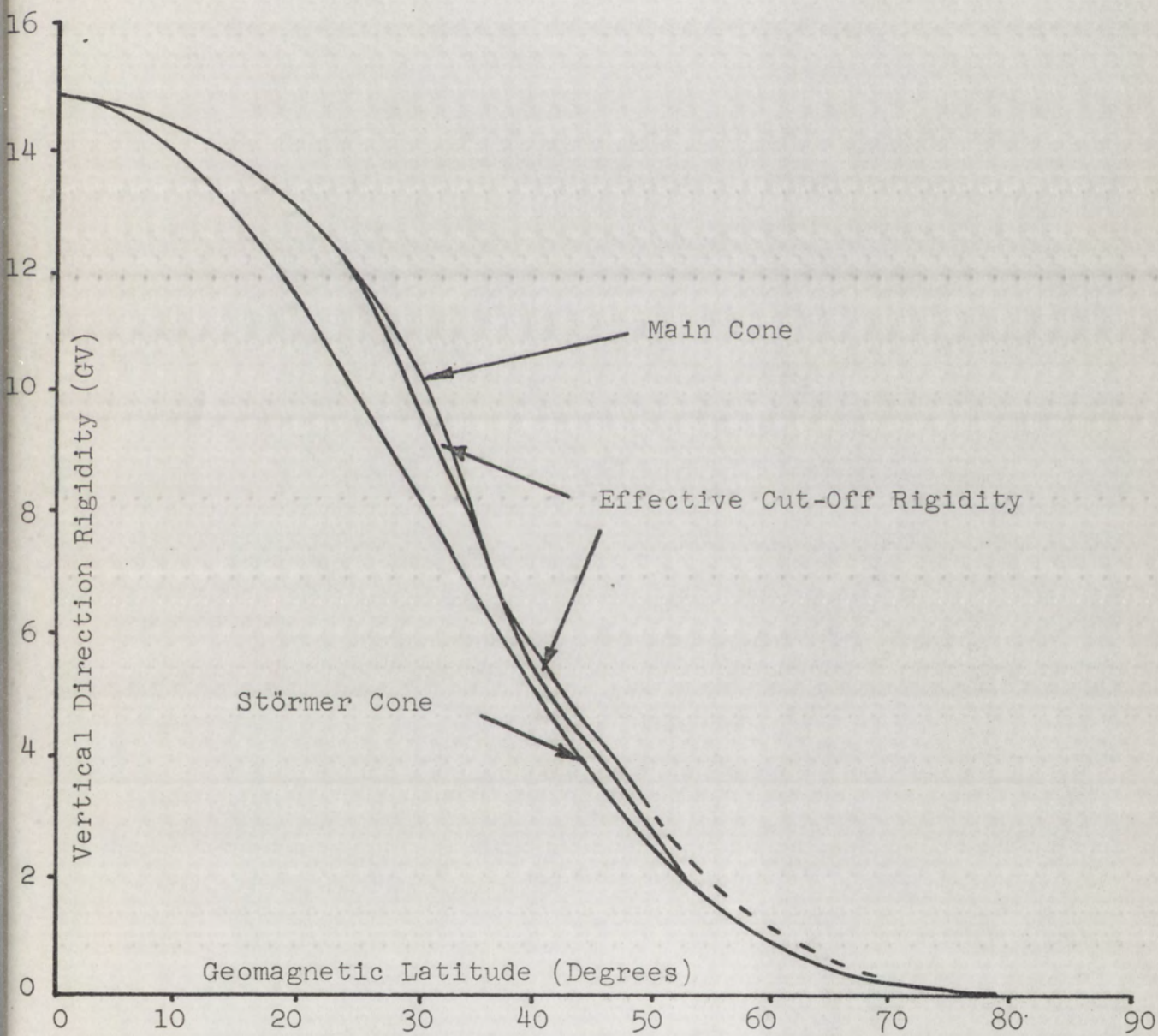


Figure 5

Simulating Curves due to Spin

Effect and Interval Read-out

5a spin period from 1.91 to 2.03 sec.

5b spin period from 0.955 to 1.015 sec.

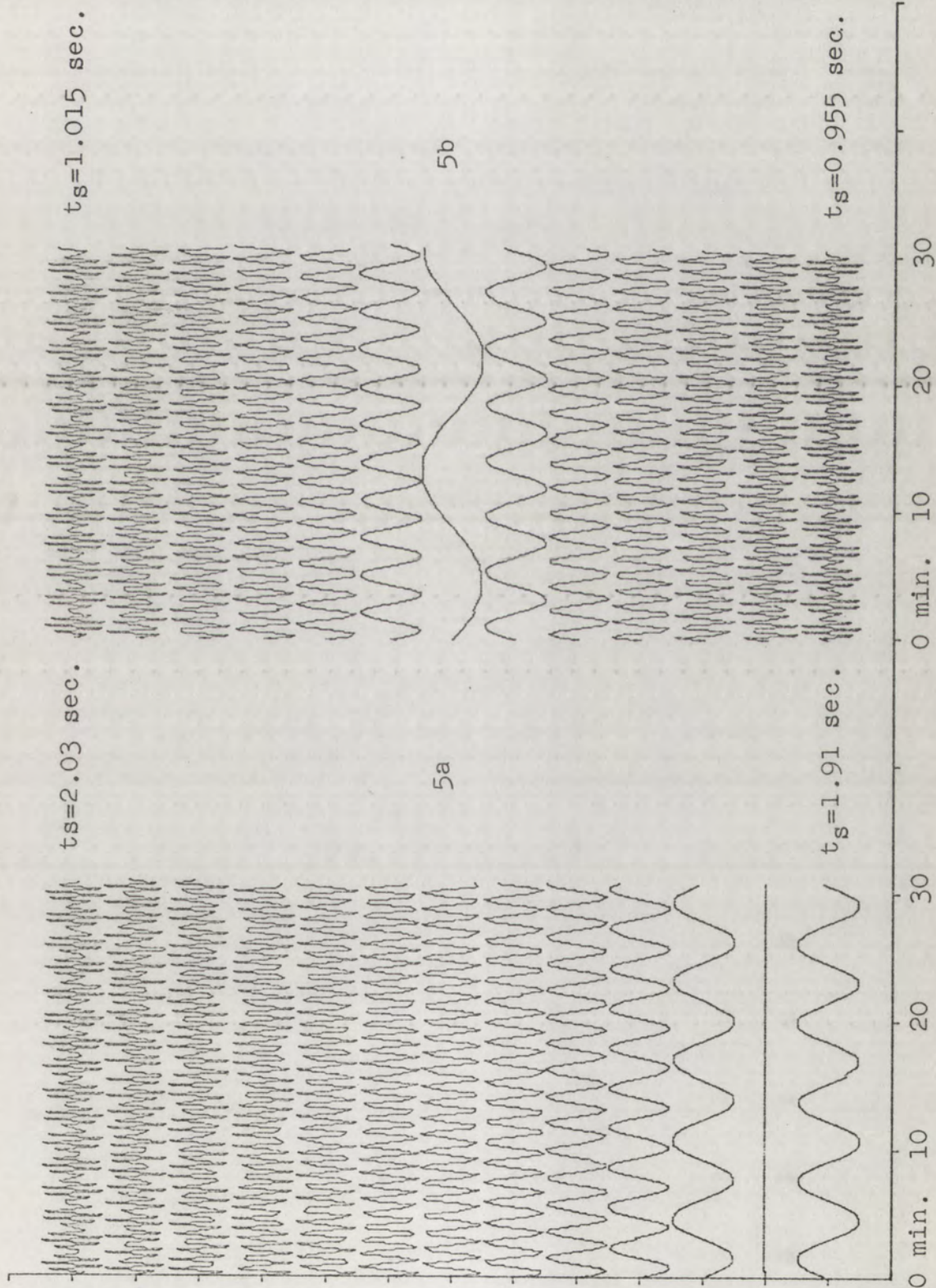


Figure 6

OSO-B2 Satellite Orbital Data

2 Lucite Cerenkov Counter (Blue)

3 Lead-glass Cerenkov Counter (Black)

4 Scintillation Counter (Red)

From	8	31965	8	1	9
To	8	31965	9	33	48

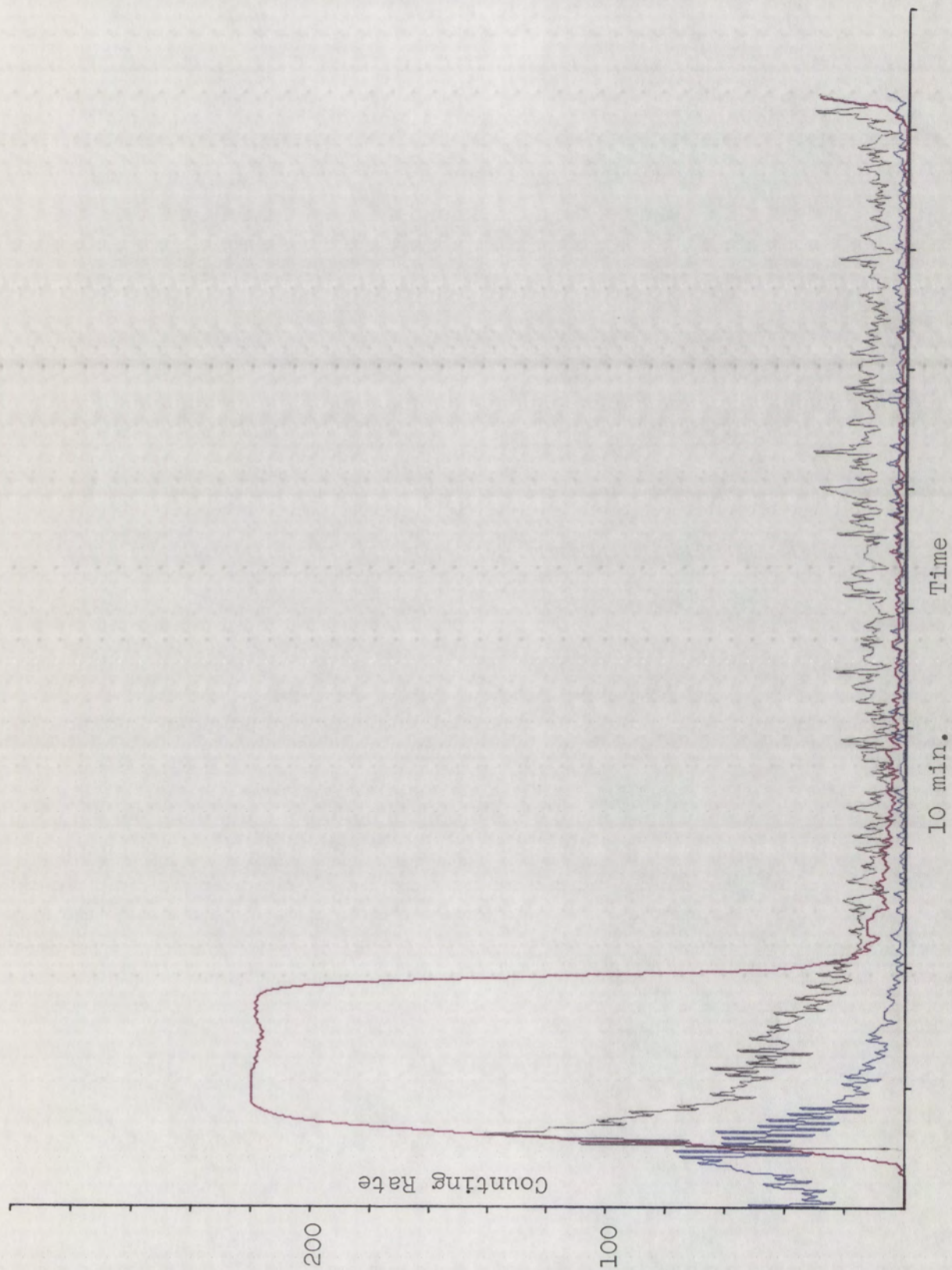


Figure 7

OSO-B2 Satellite Orbital Data

2 Lucite Cerenkov Counter (Blue)

3 Lead-glass Cerenkov Counter (Black)

4 Scintillation Counter (Red)

From	4	271965	20	3	41
To	4	271965	21	40	7

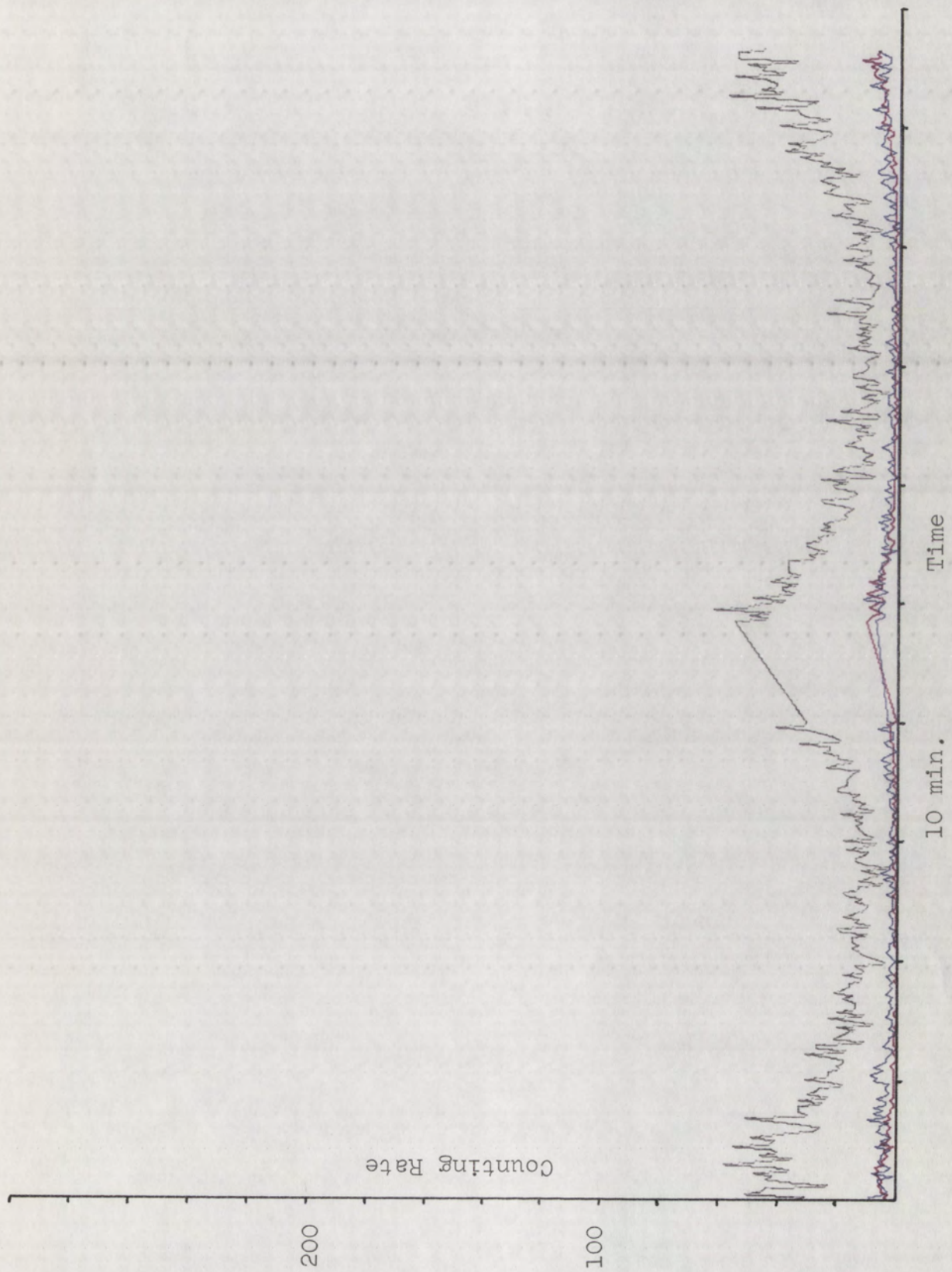


Figure 8

OSO-B2 Satellite Orbital Data

- 2 Lucite Cerenkov Counter (Blue)
- 3 Lead-glass Cerenkov Counter (Black)
- 4 Scintillation Counter (Red)

From	6	41965	9	41	5
To	6	41965	11	8	21

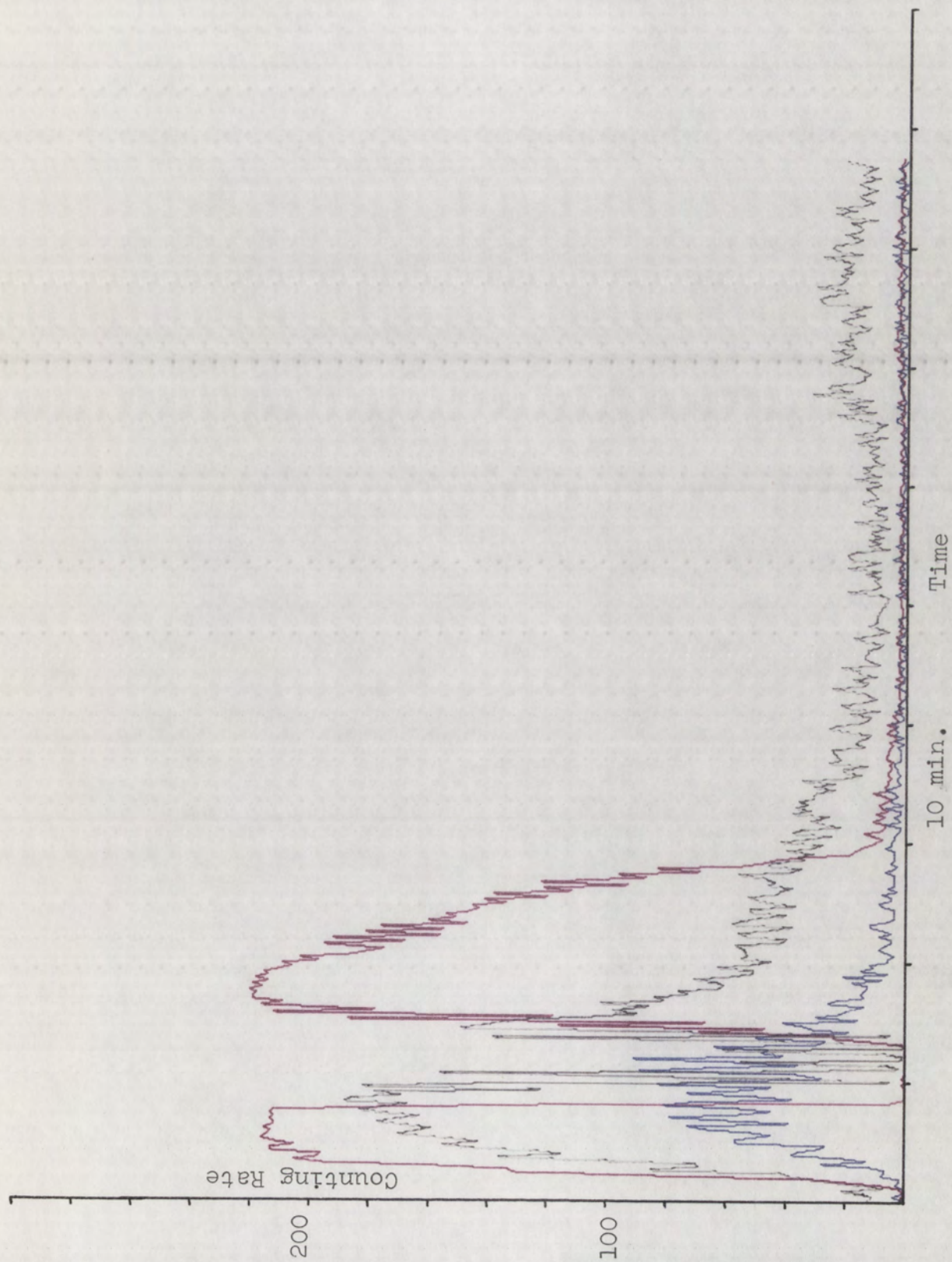


Figure 9

OSO-B2 Satellite Orbital Data

2 Lucite Cerenkov Counter (Blue)

3 Lead-glass Cerenkov Counter (Black)

4 Scintillation Counter (Red)

From	6	41965	7	55	24
To	6	41965	9	29	50

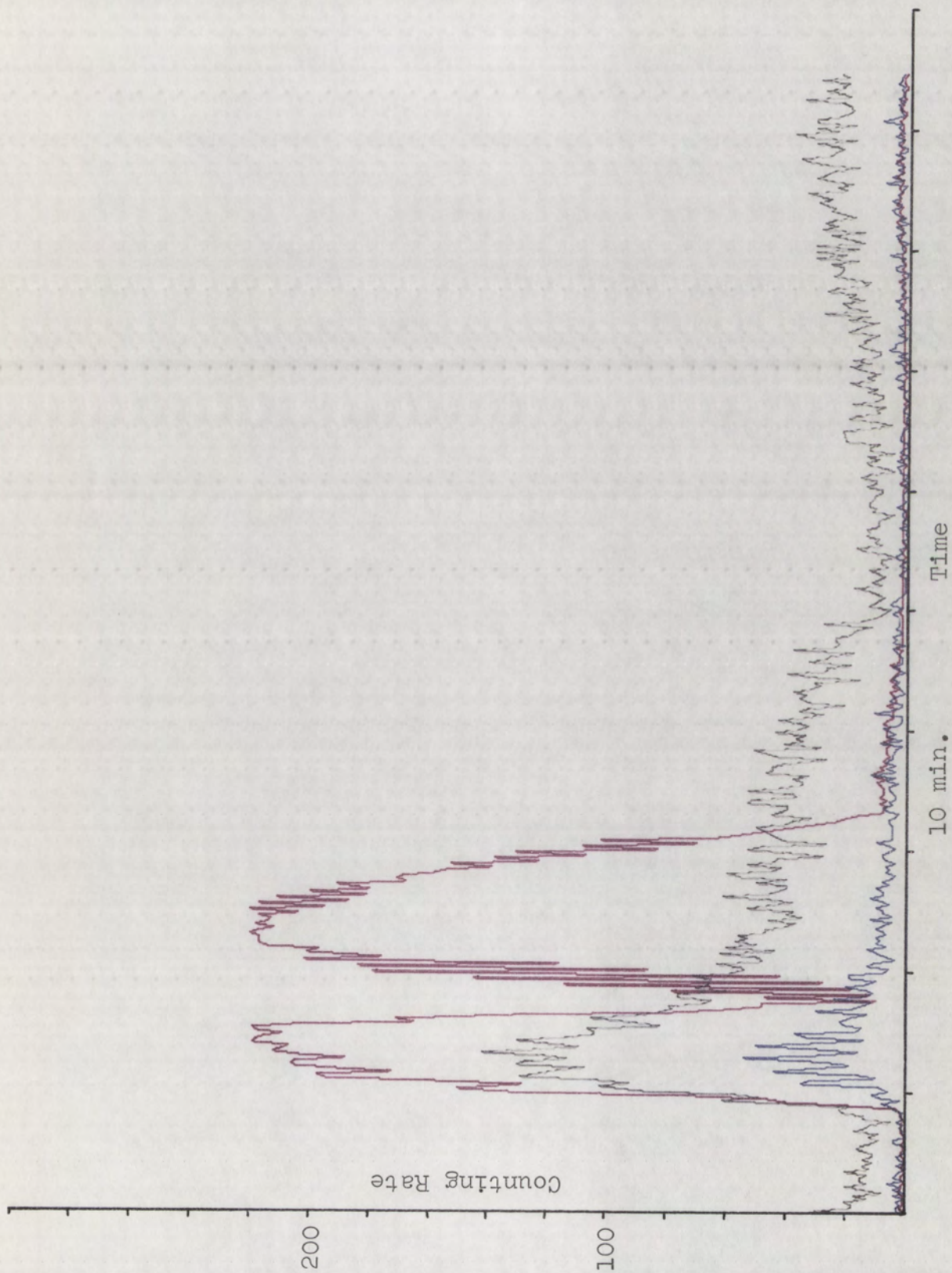


Figure 10

OSO-B2 Satellite Orbital Data

2 Lucite Cerenkov Counter (Blue)

3 Lead-glass Cerenkov Counter

4 Scintillation Counter (Red)

From	8	161965	18	59	41
To	8	161965	20	36	7

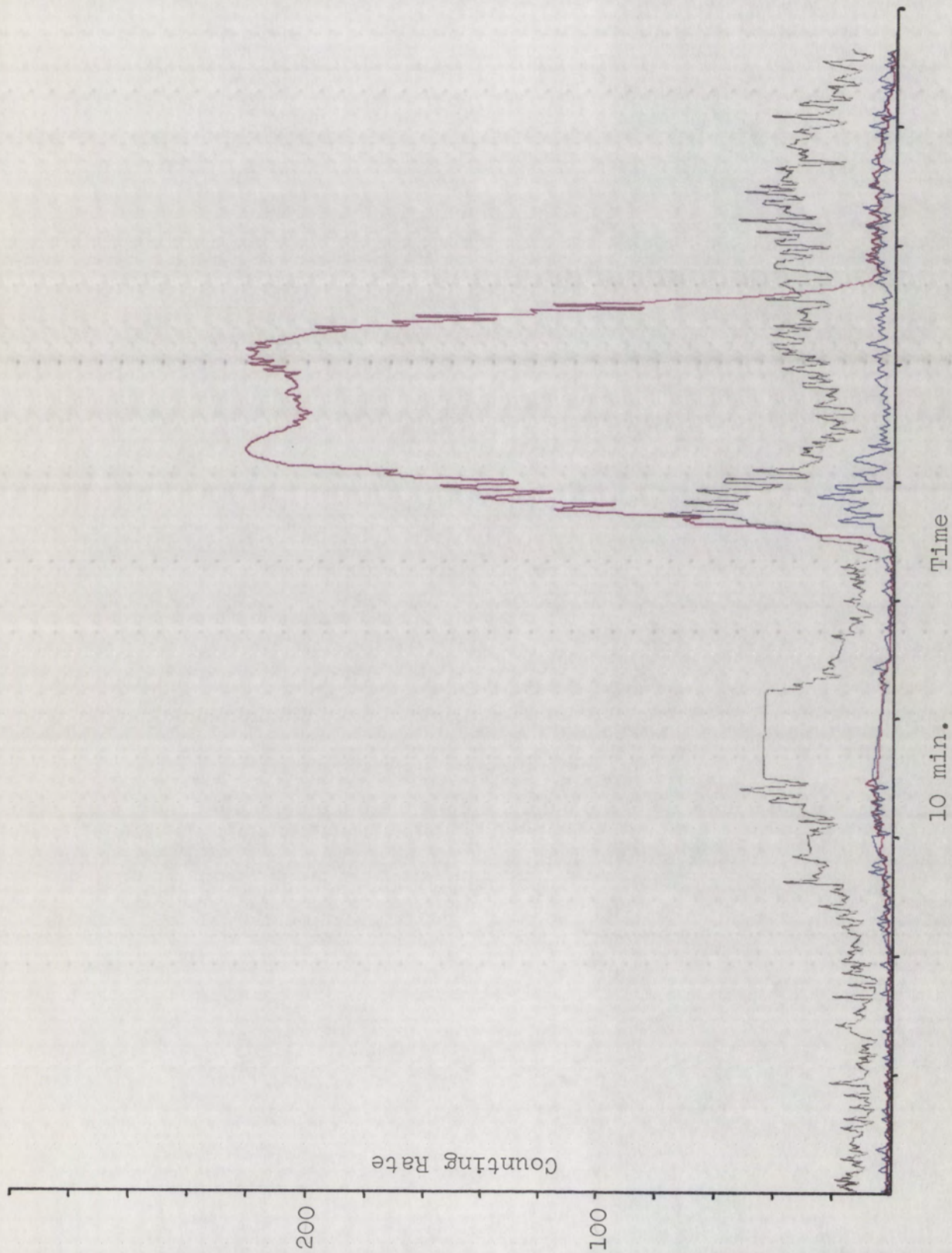


Figure 11

OSO-B2 Satellite Orbital Data

- 2 Lucite Cerenkov Counter (Blue)
- 3 Lead-glass Cerenkov Counter (Black)
- 4 Scintillation Counter (Red)

From	8	161965	20	36	23
To	8	161965	22	12	34

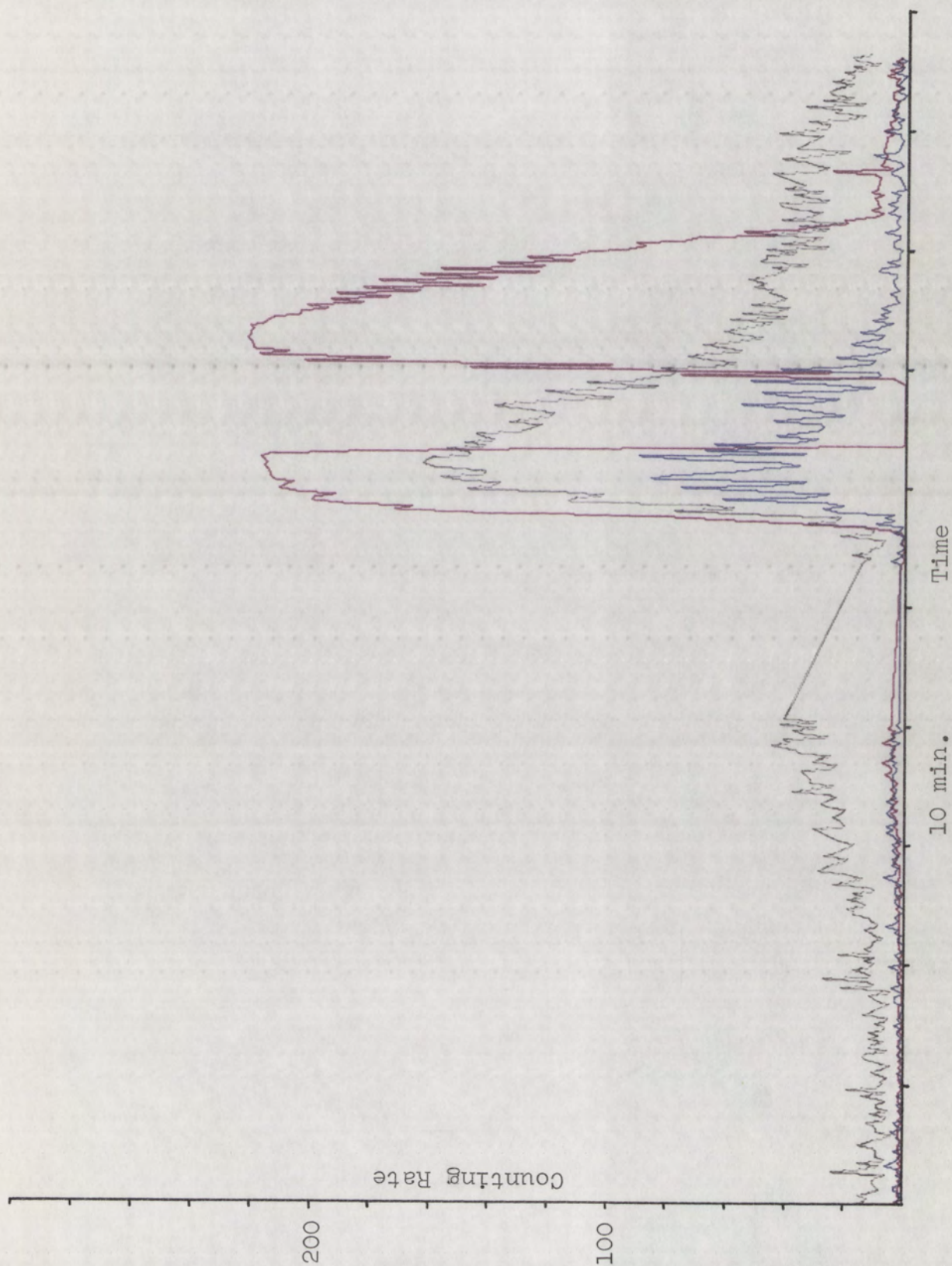


Figure 12

Flux Intensity as a Function of Time

(From February 5 to July 31)

at -120° longitude and 0° latitude

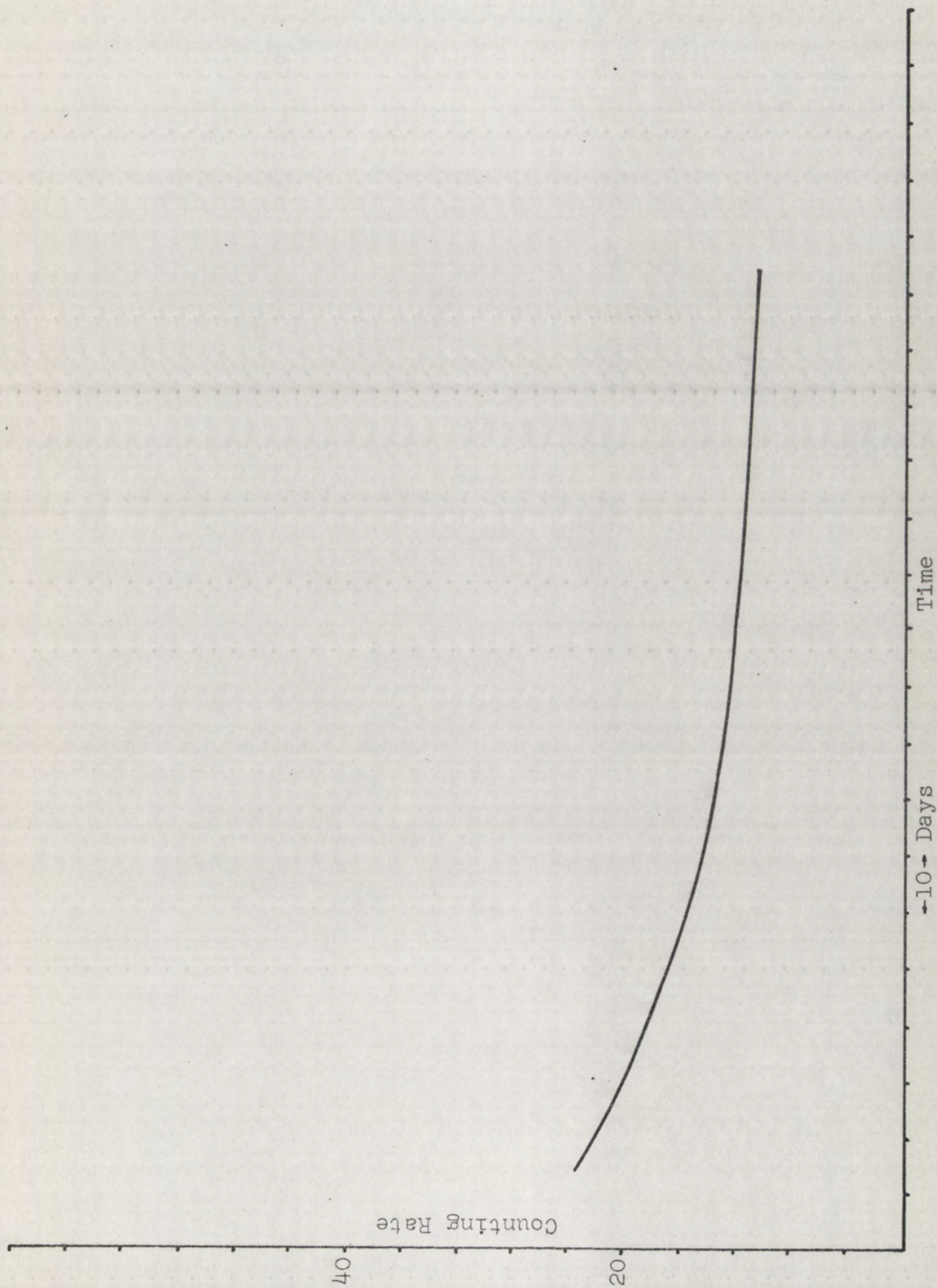


Figure 13

Flux Intensity as a Function of Time

(From February 5 to July 31)

at 90° longitude and 0° latitude

Counting Rate

40

20

Time

-10- Days

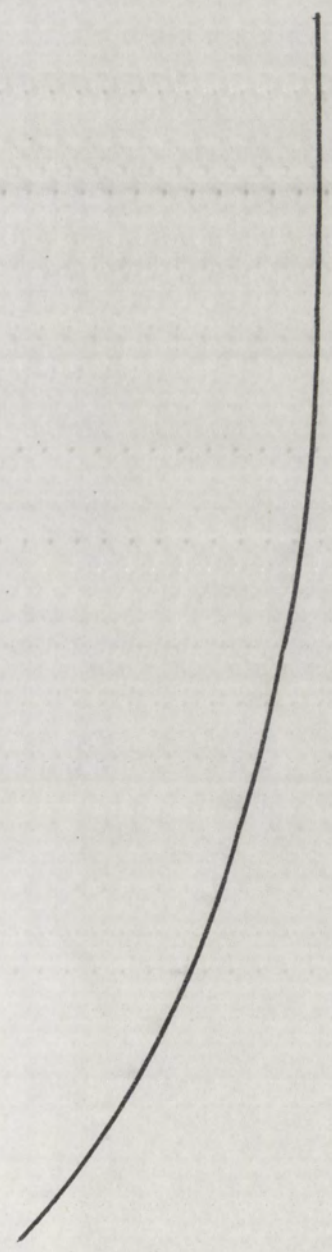


Figure 14

Geographic Longitude Effect

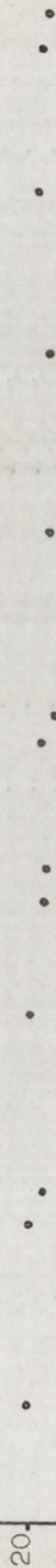
(a) Geographic Longitude vs. Counting Rate

March 2

(b) Geographic Longitude vs. Counting Rate

March 15

Mar. 2



Mar. 15

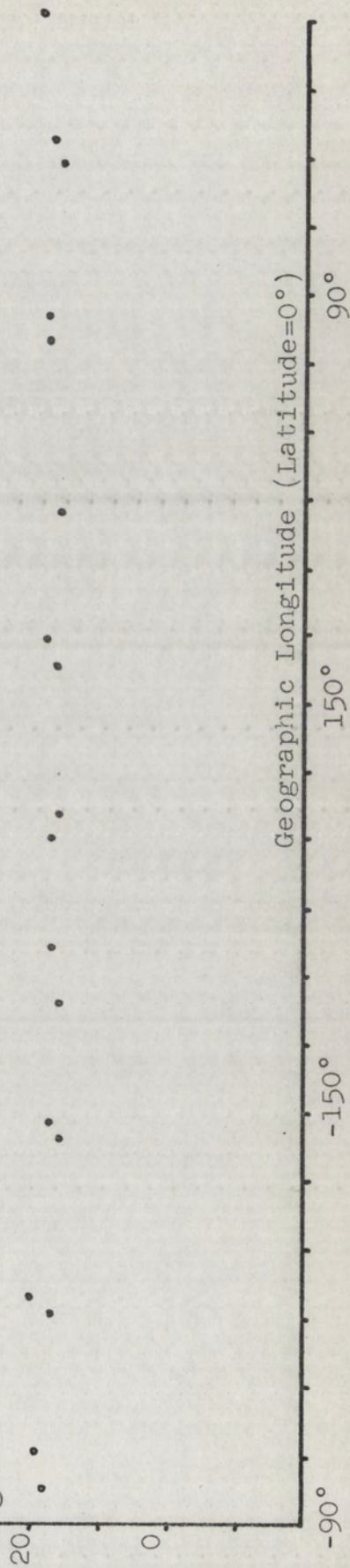


Figure 15

Geographic Latitude Effect

(a) Geographic Latitude vs. Counting Rate

March 16

(b) Geographic Latitude vs. Counting Rate

June 4

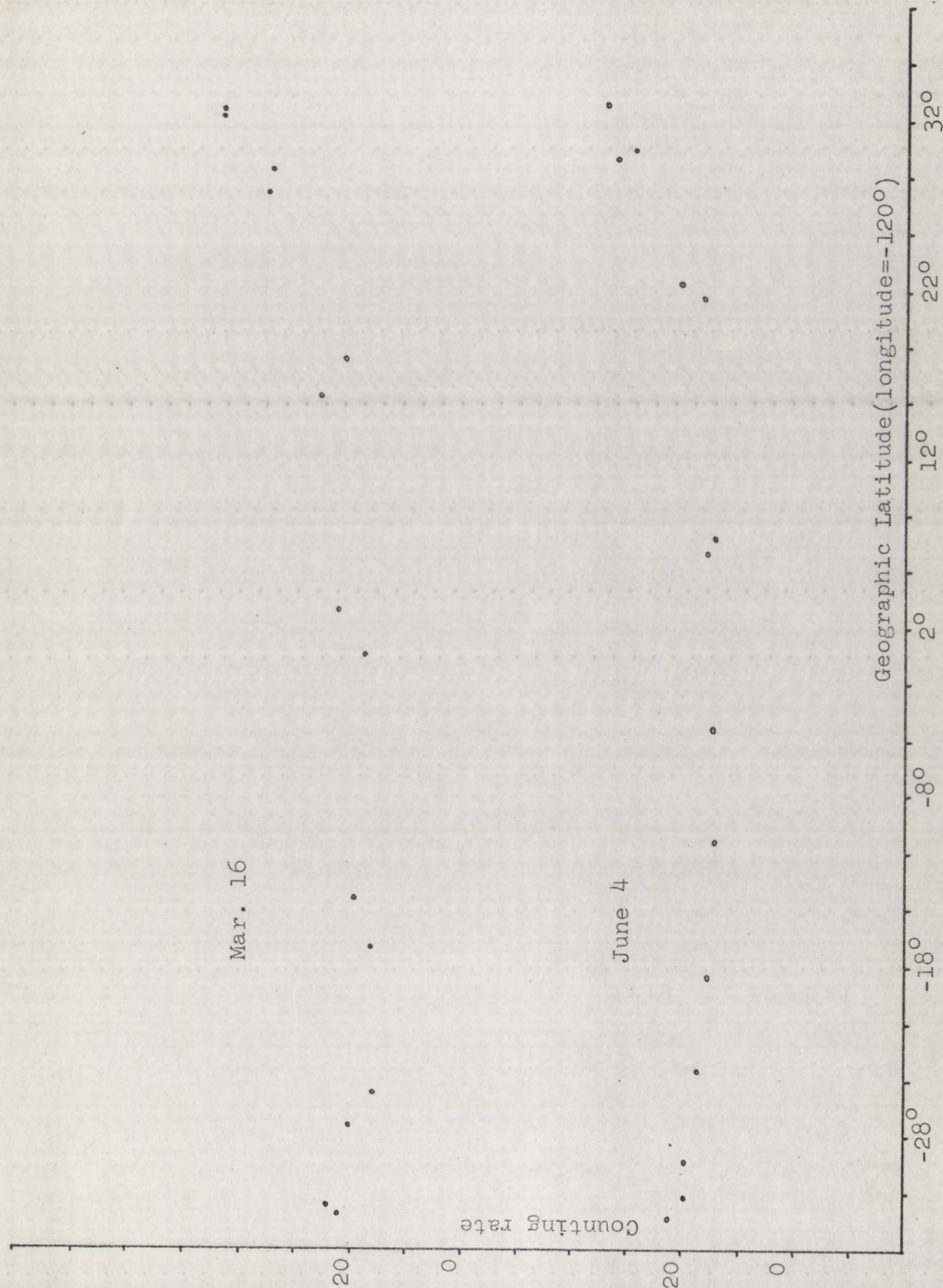
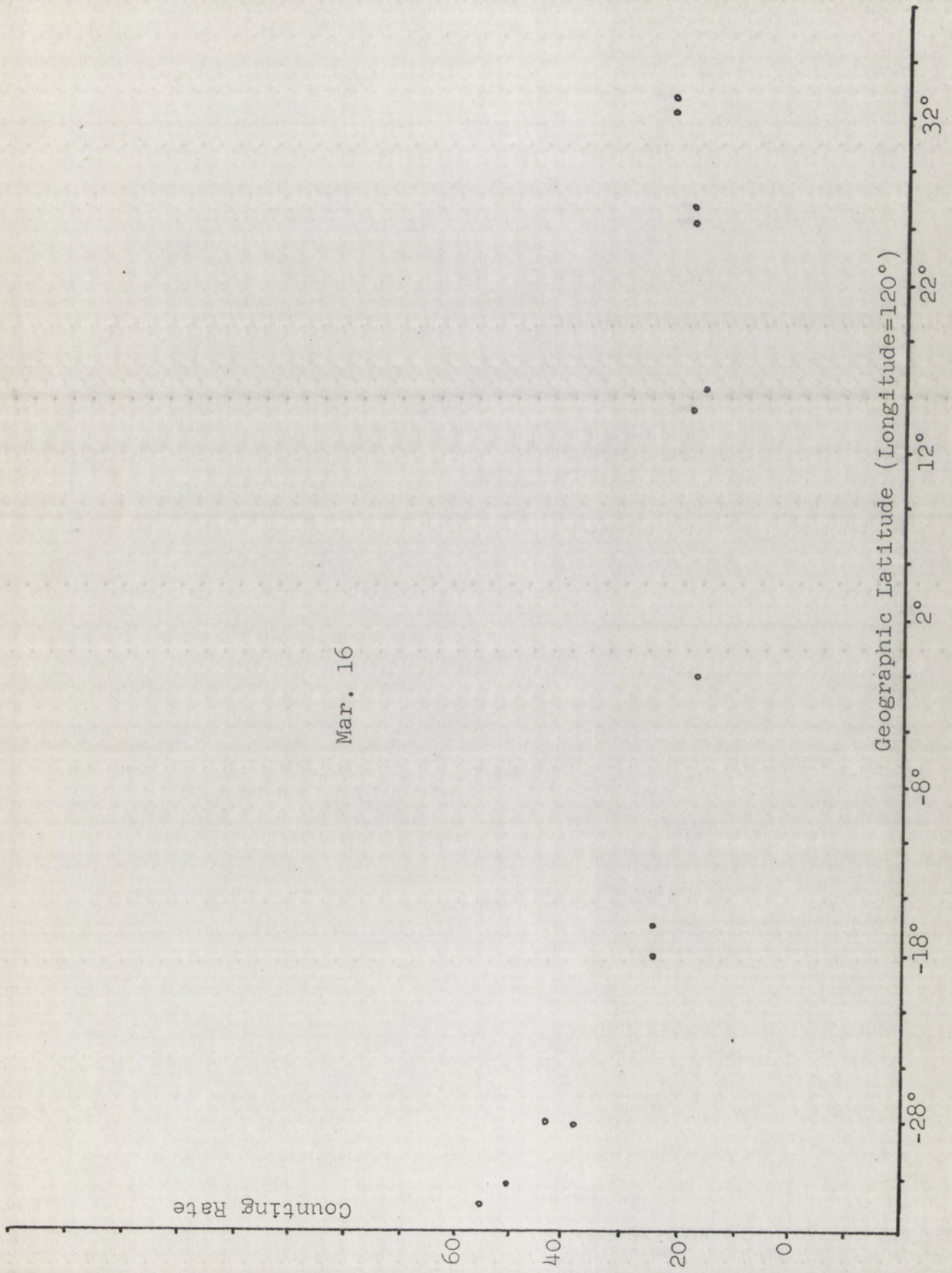


Figure 16

Geographic Latitude Effect

Geographic Latitude vs. Counting Rate

Mar. 16



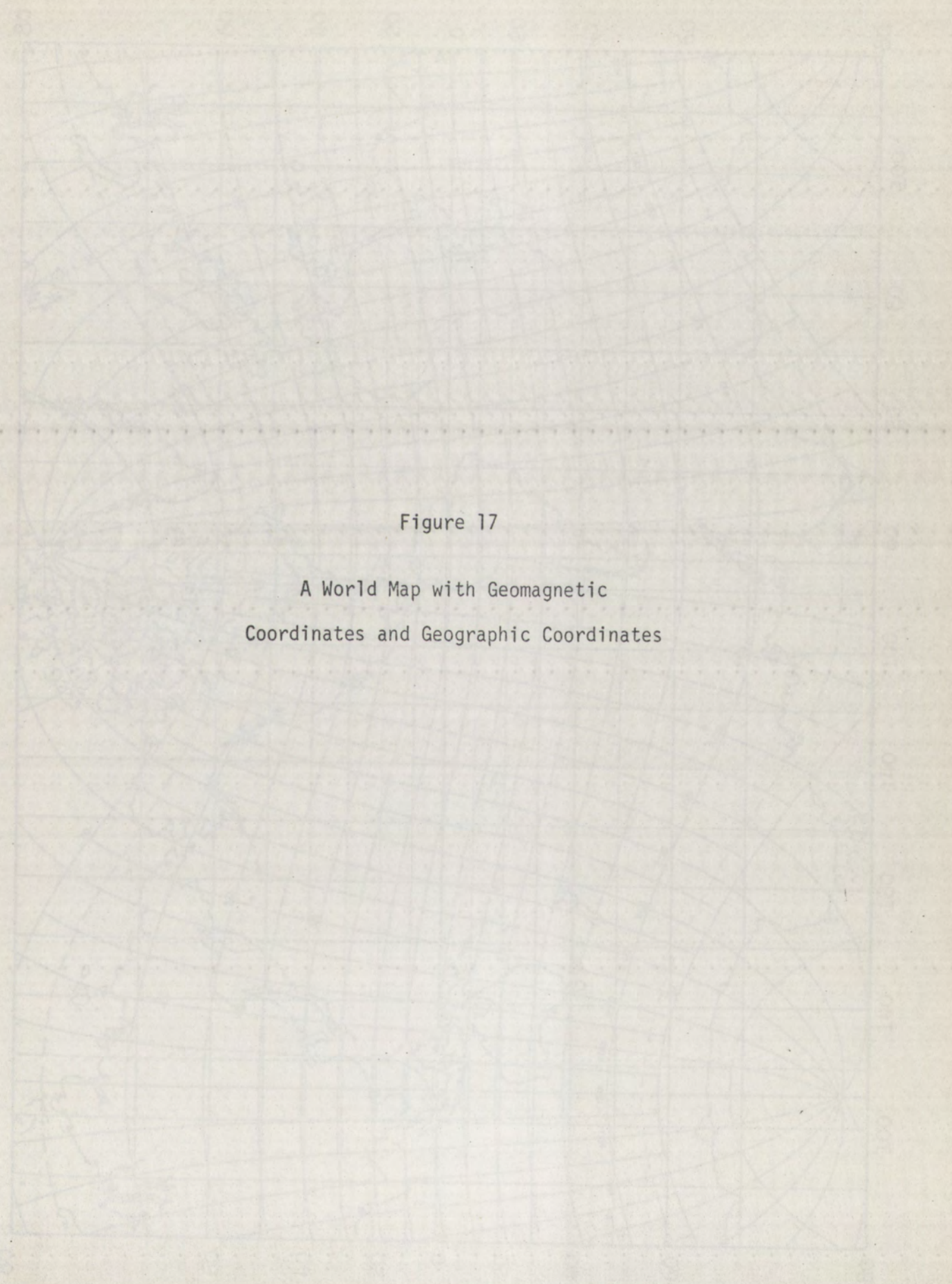


Figure 17

A World Map with Geomagnetic
Coordinates and Geographic Coordinates

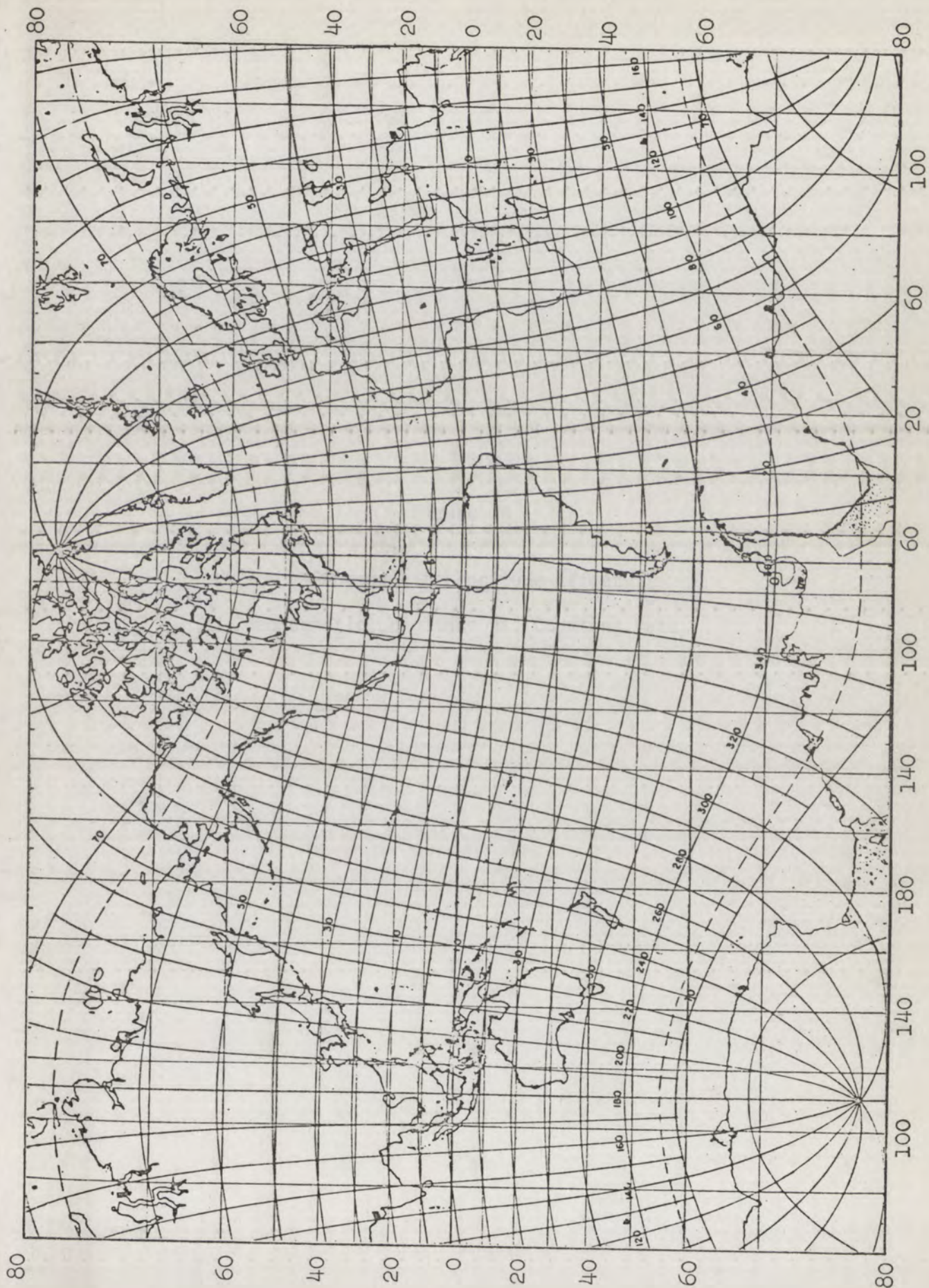


Figure 18

Geomagnetic Longitude Effect

Geomagnetic Longitude vs. Counting Rate

Counting Rate

Geomagnetic Longitude (Latitude=0°)

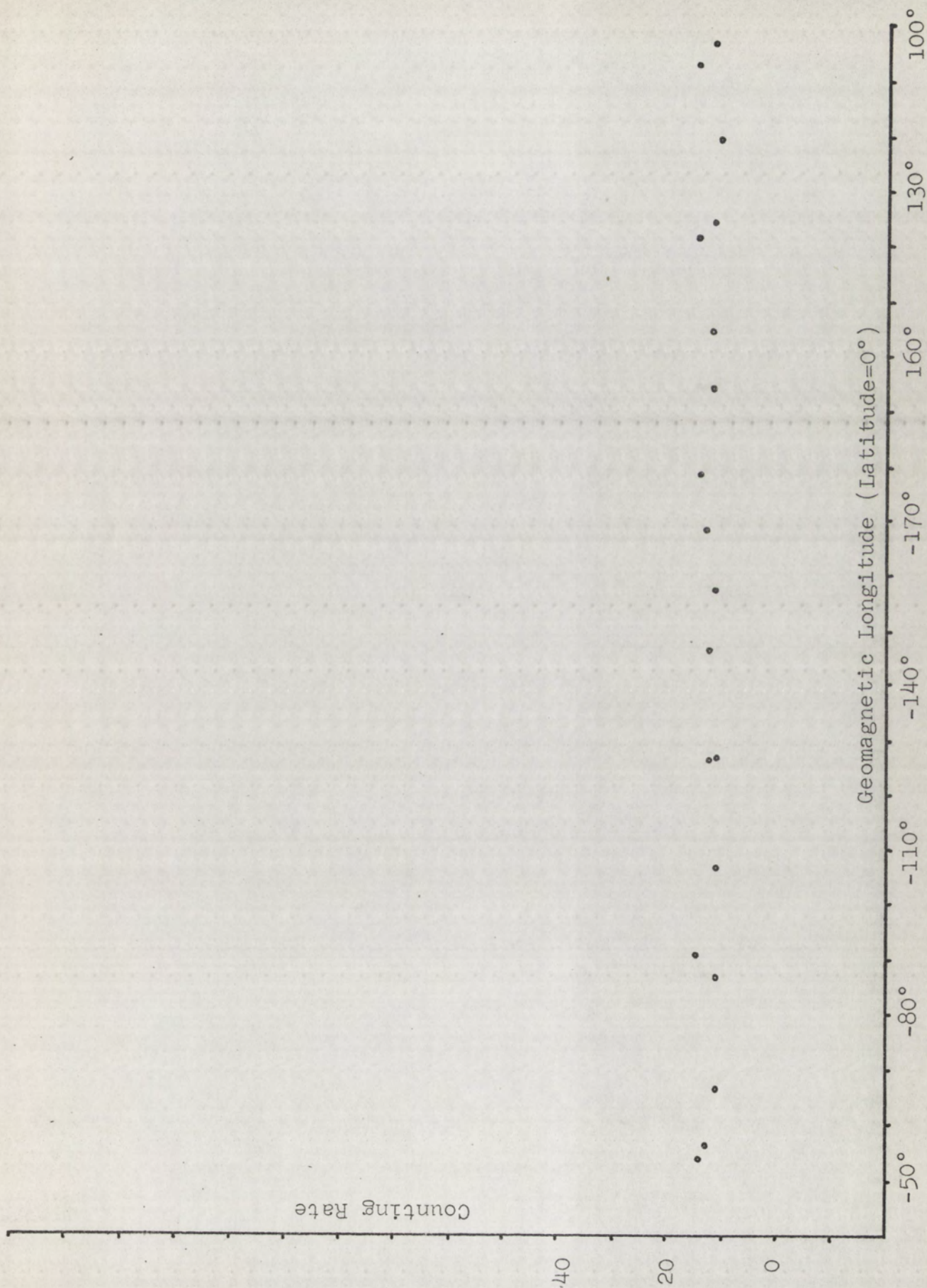


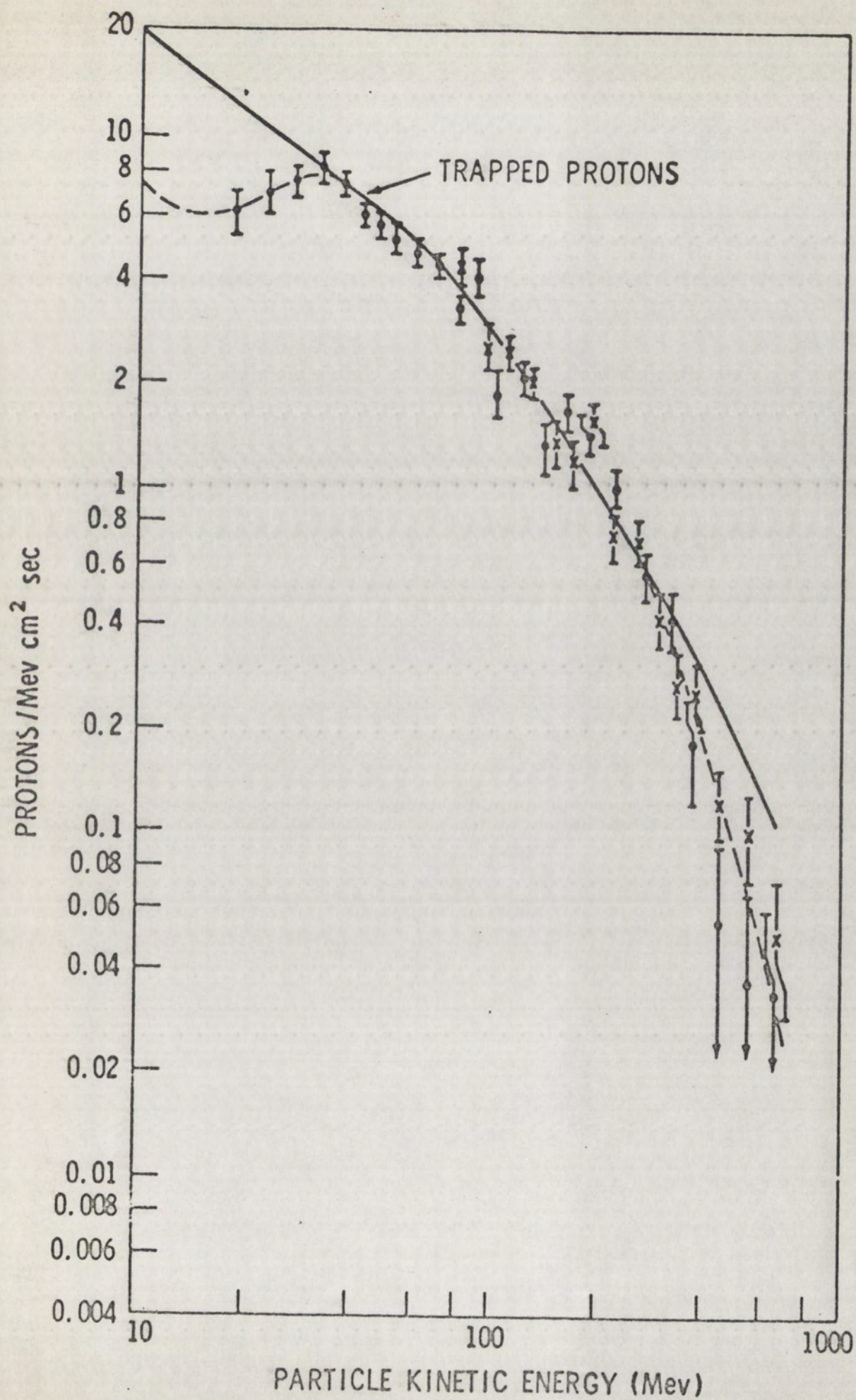
Figure 19

Geomagnetic Latitude Effect

Geomagnetic Latitude vs. Counting Rate

Figure 20

An Energy Spectrum of Proton in the SARA



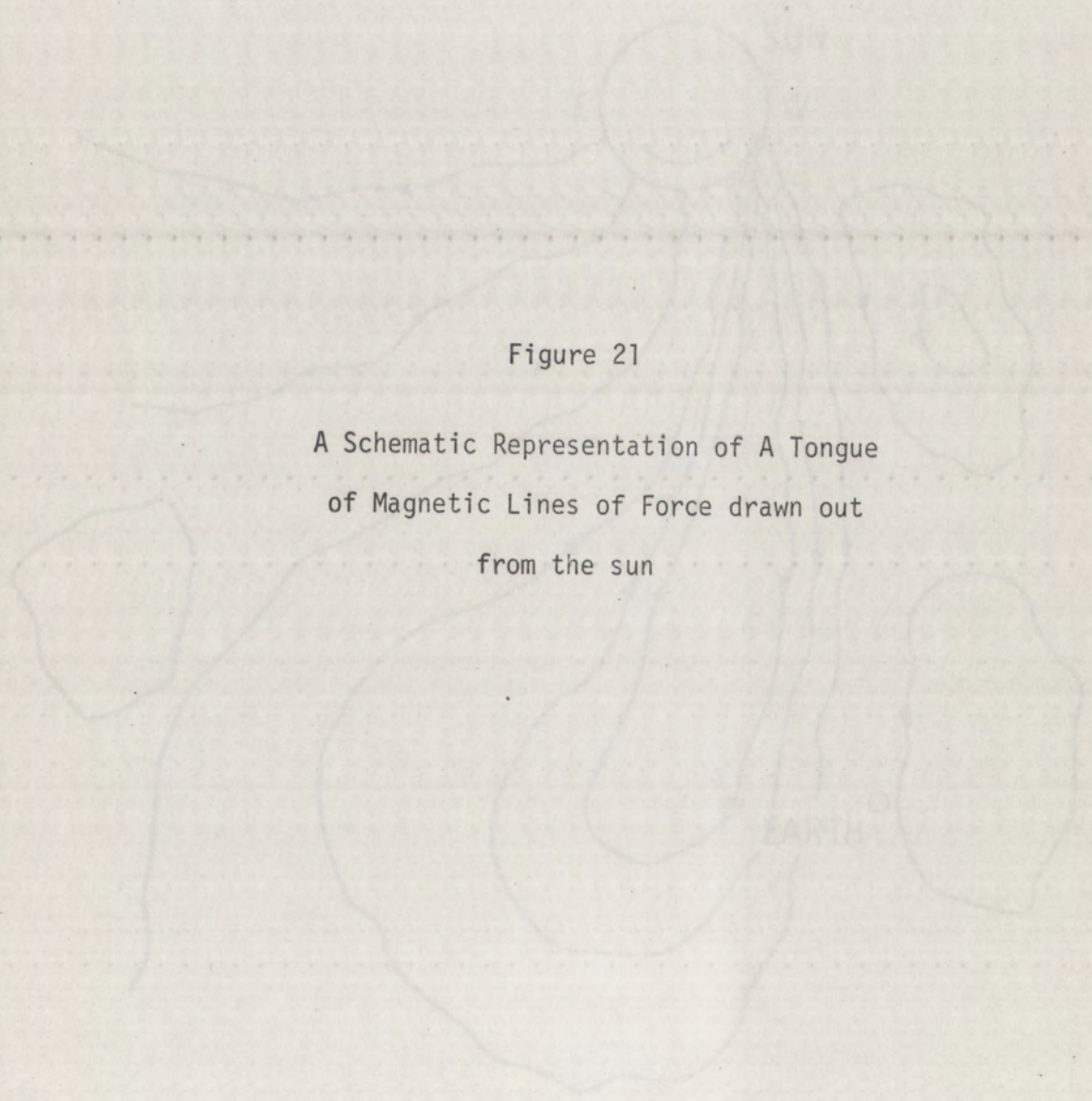
A schematic diagram showing a large, irregular, cloud-like shape representing a 'tongue' of magnetic lines of force. This shape is elongated and has several smaller, rounded protrusions. In the center of this large shape, there is a smaller, more circular area. To the right of this central area, the word 'EARTH' is written in a simple, sans-serif font. The entire diagram is drawn with thin, light blue lines on a plain, off-white background.

Figure 21

A Schematic Representation of A Tongue
of Magnetic Lines of Force drawn out
from the sun

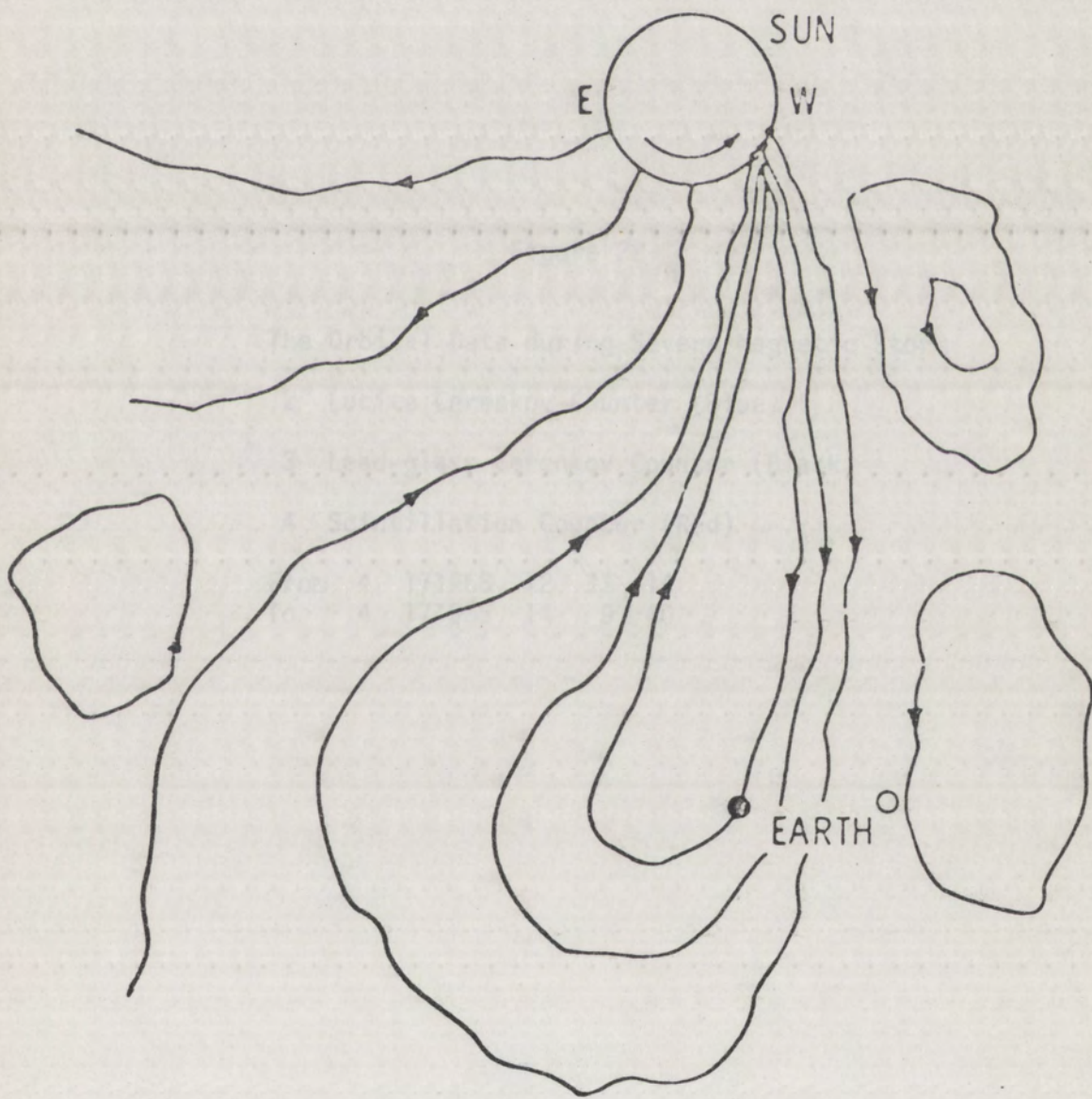


Figure 22

The Orbital Data during Severe Magnetic Storm

2 Lucite Cerenkov Counter (Blue)

3 Lead-glass Cerenkov Counter (Black)

4 Scintillation Counter (Red)

From	4	171965	12	33	14
To	4	171965	14	9	40

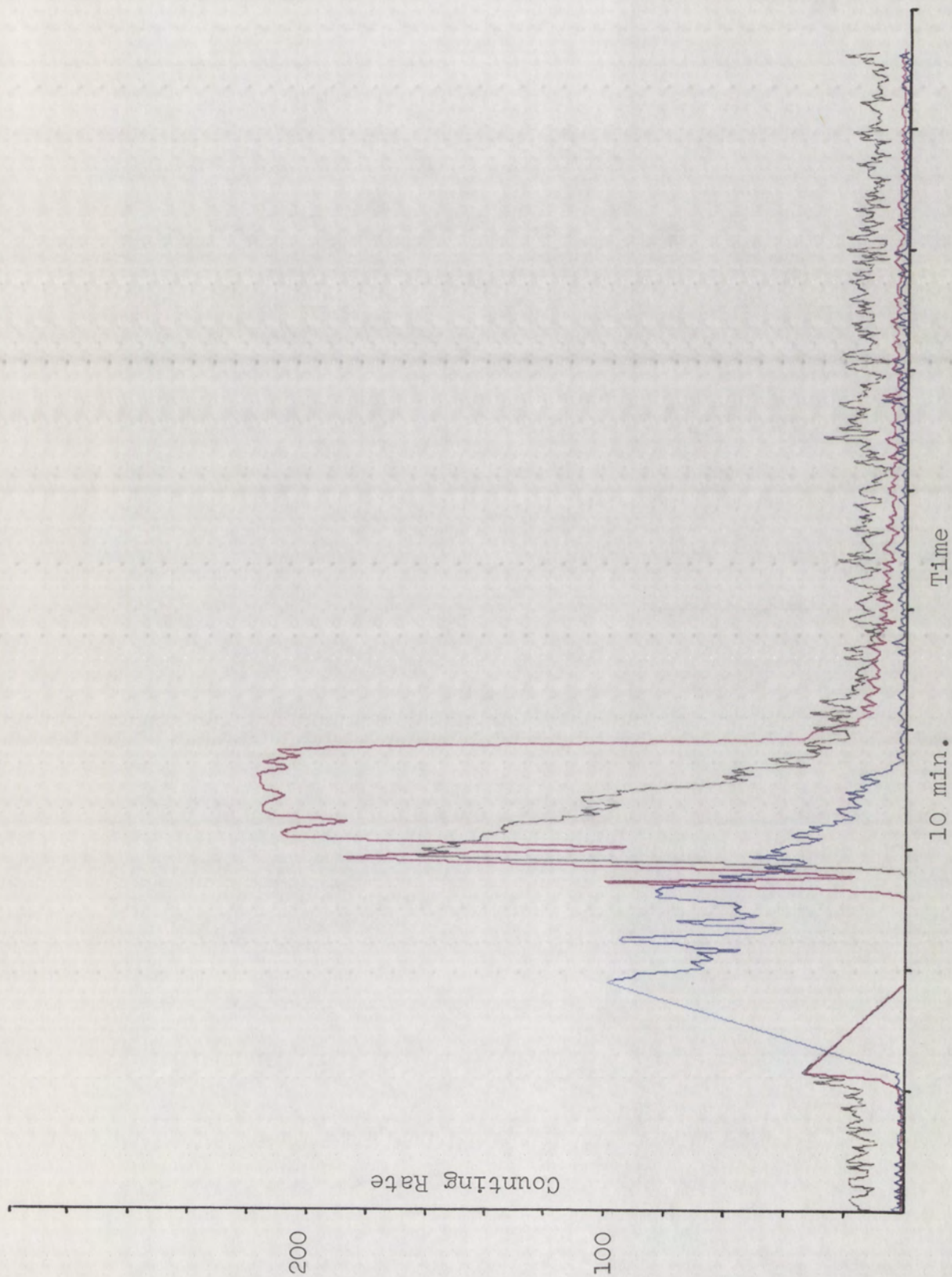


Figure 23

The Orbital Data during Severe Magnetic Storm

2 Lucite Cerenkov Counter (Blue)

3 Lead-glass Cerenkov Counter (Black)

4 Scintillation Counter (Red)

From	4	171965	14	9	55
To	4	171965	15	45	35

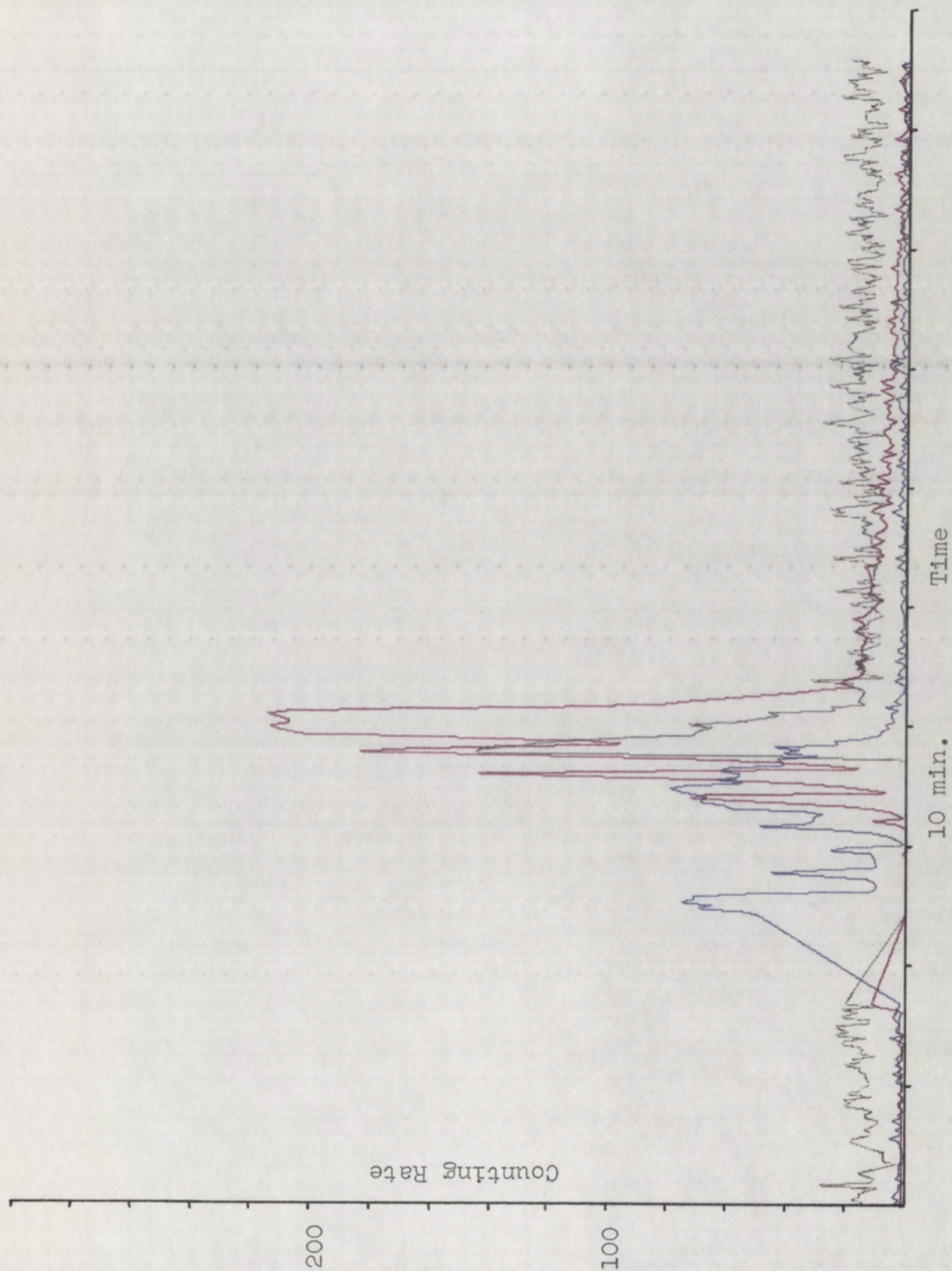


Figure 24

The Orbital Data during Severe Magnetic Storm

2 Lucite Cerenkov Counter (Blue)

3 Lead-glass Cerenkov Counter (Black)

4 Scintillation Counter (Red)

From	4	171965	15	45	51
To	4	171965	17	22	33

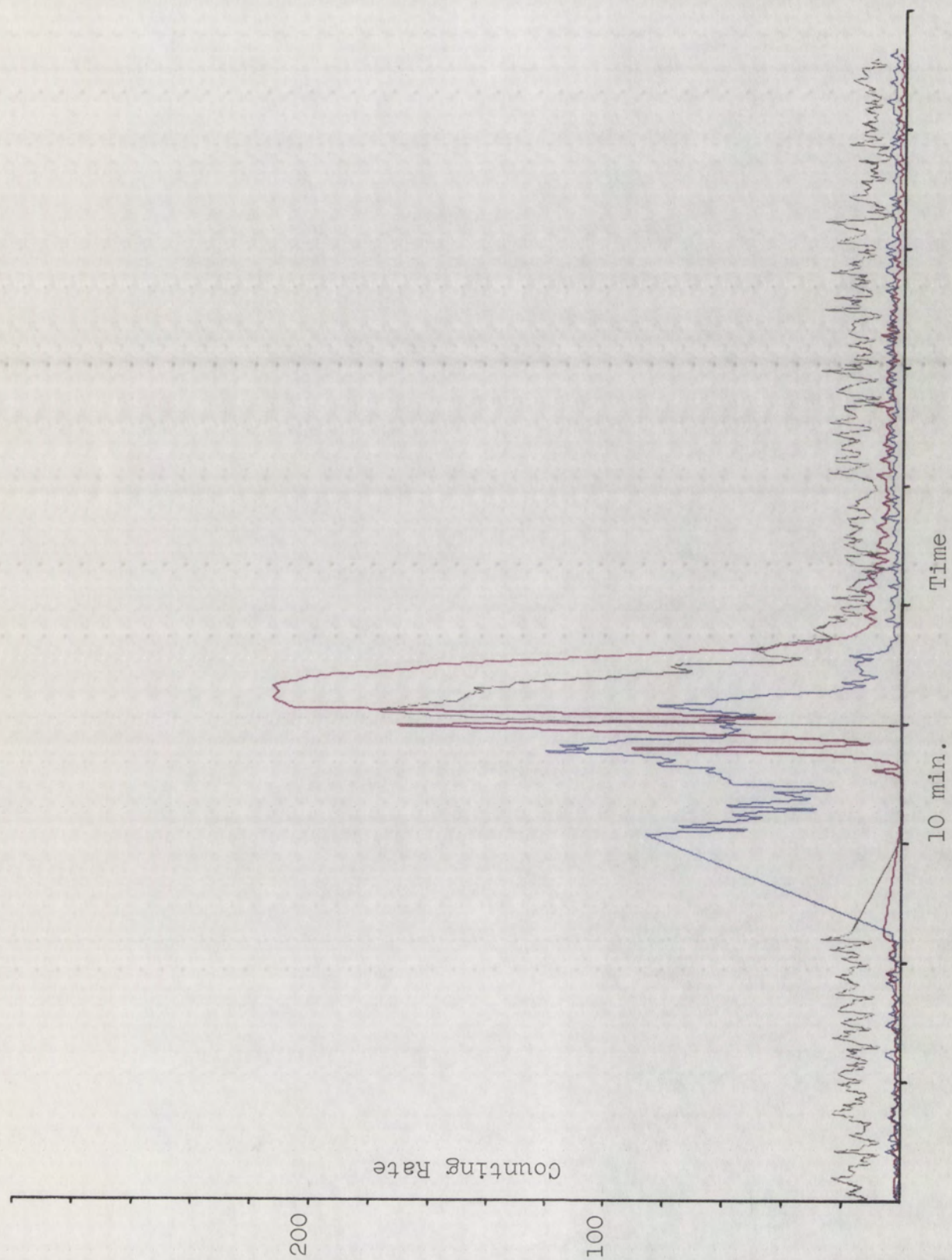


Figure 25

The Orbital Data during Severe Magnetic Storm

2 Lucite Cerenkov Counter (Blue)

3 Lead-glass Cerenkov Counter (Black)

4 Scintillation Counter (Red)

From	4	171965	17	22	48
To	4	171965	18	58	28

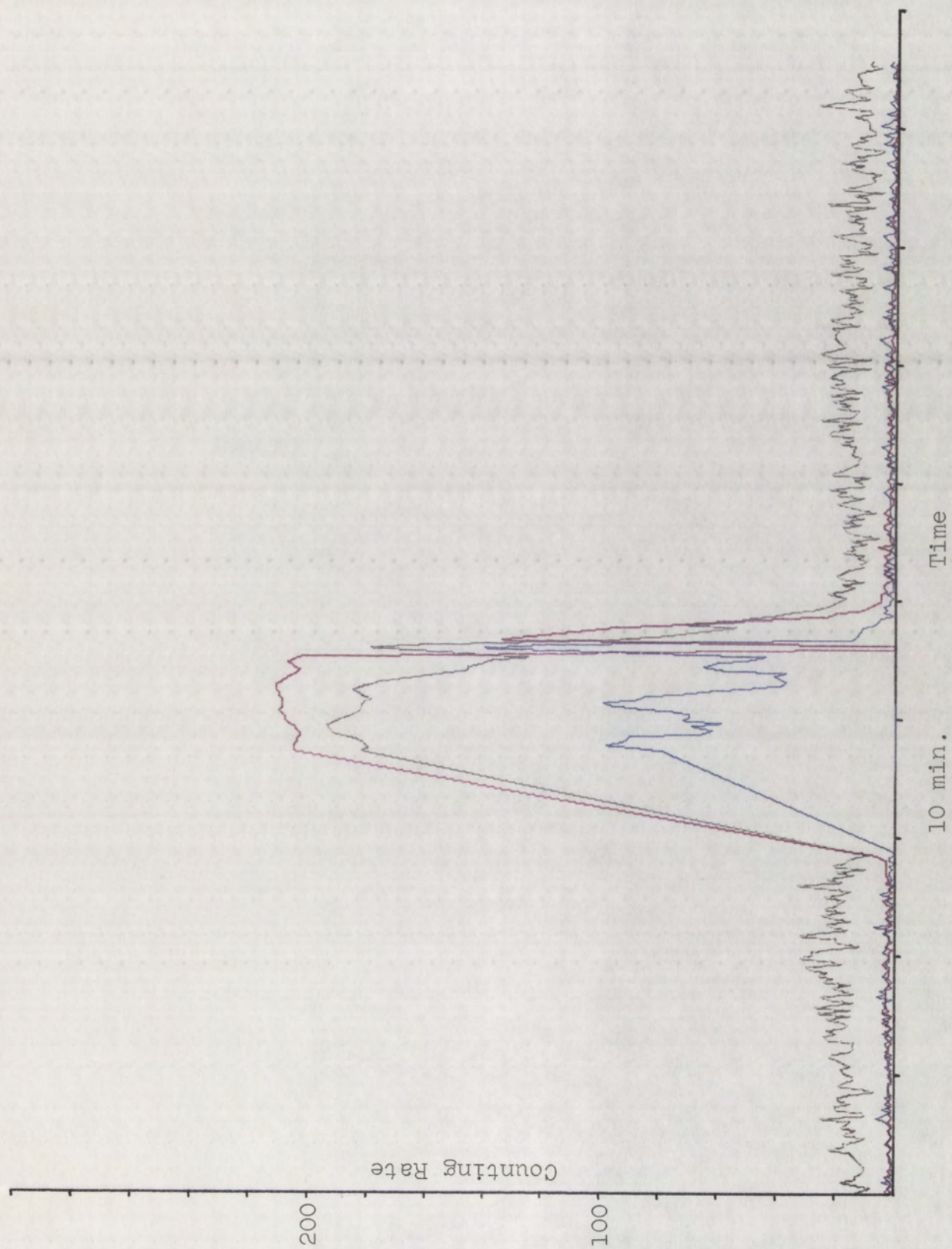


Figure 26

Orbital Data with the Same Tracks as Figure 22

2 Lucite Cerenkov Counter (Blue)

3 Lead-glass Cerenkov Counter (Black)

4 Scintillation Counter (Red)

From	4	111965	15	19	24
To	4	111965	16	55	50

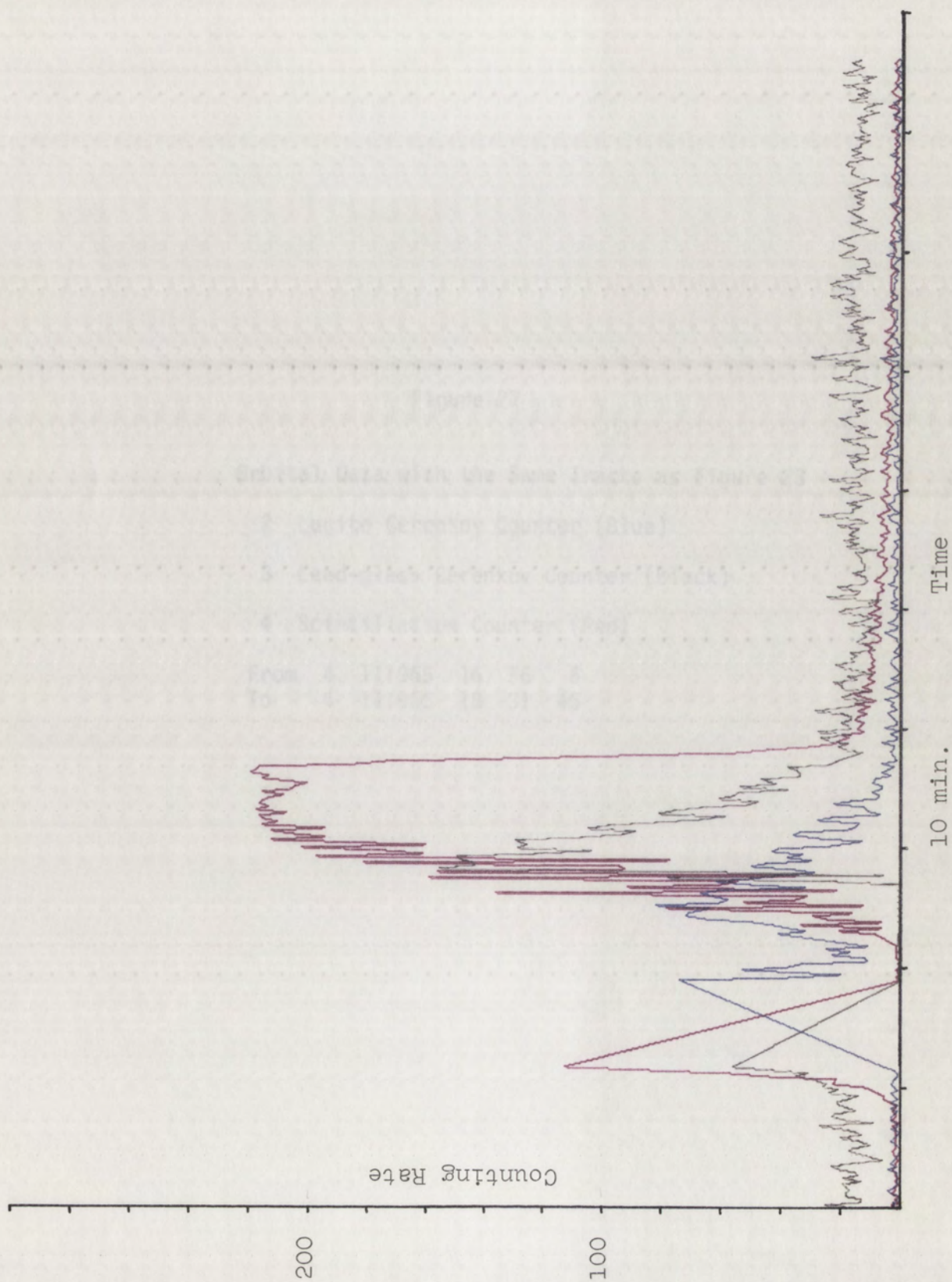


Figure 27

Orbital Data with the Same Tracks as Figure 23

2 Lucite Cerenkov Counter (Blue)

3 Lead-glass Cerenkov Counter (Black)

4 Scintillation Counter (Red)

From	4	111965	16	56	6
To	4	111965	18	31	45

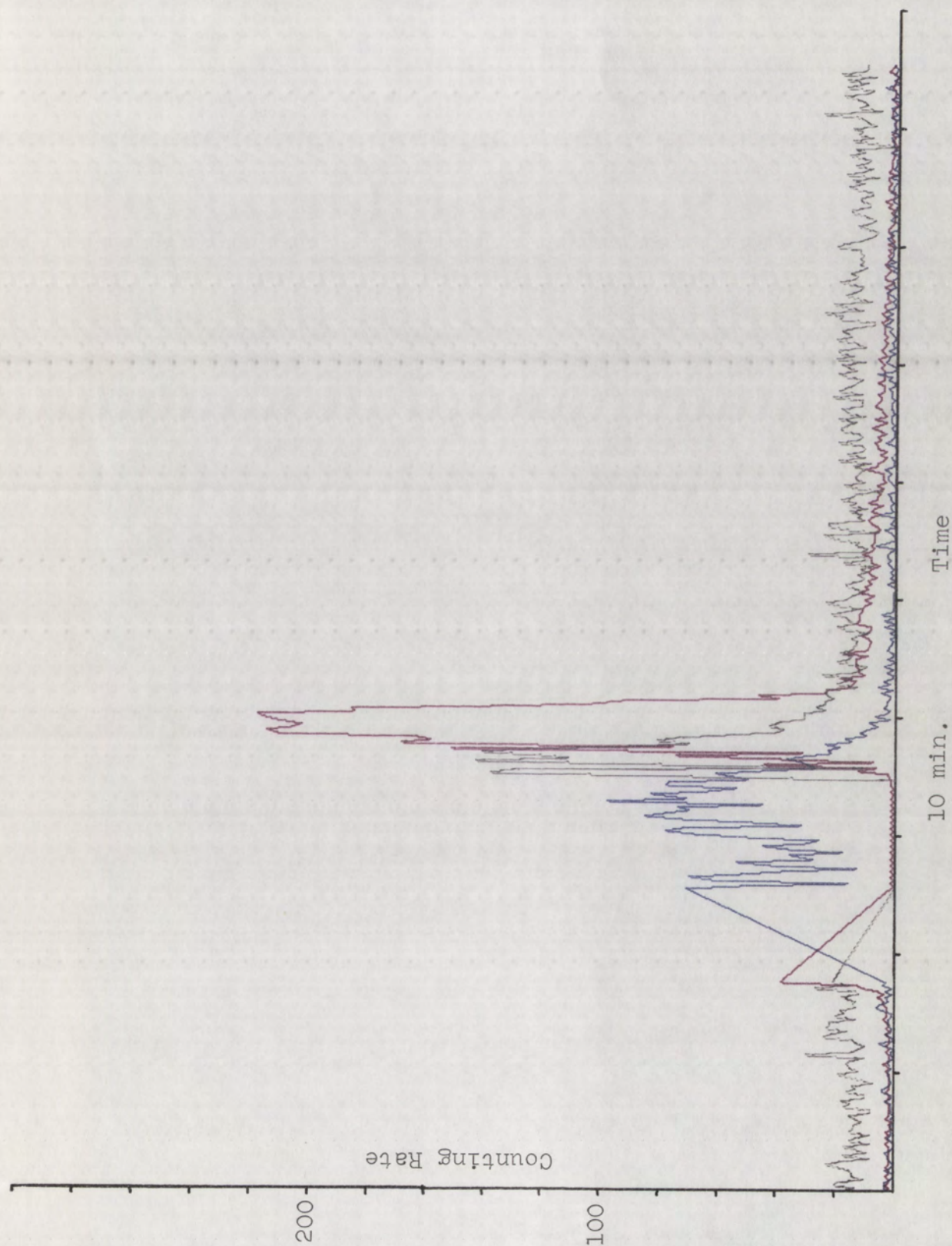


Figure 28

Orbital Data with the Same Tracks as Figure 24

2 Lucite Cerenkov Counter (Blue)

3 Lead-glass Cerenkov Counter (Black)

4 Scintillation Counter (Red)

From	4	111965	18	32	7
To	4	111965	20	8	43

